NUREG-1726

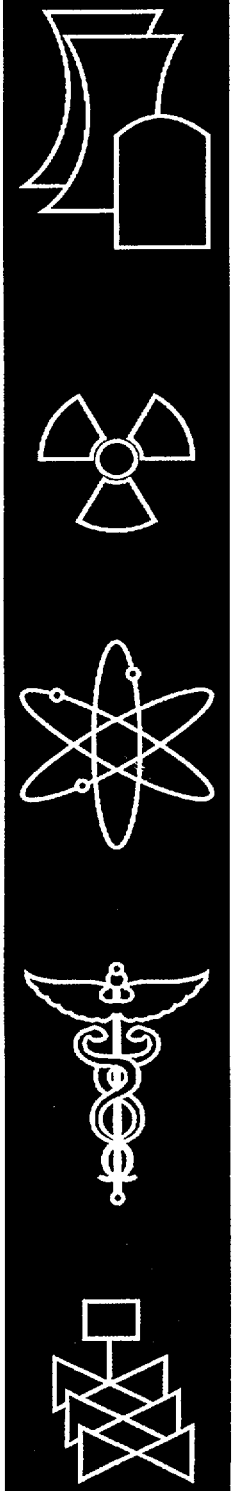

Predictions of Spent Fuel Heatup After a Complete Loss of Spent Fuel Pool Coolant

U.S. Nuclear Regulatory Commission
Office Nuclear Regulatory Research
Washington, DC 20555-0001

AVAILABILITY OF REFERENCE MATERIALS IN NRC PUBLICATIONS

NRC Reference Material

As of November 1999, you may electronically access NUREG-series publications and other NRC records at NRC's Public Electronic Reading Room at www.nrc.gov/NRC/ADAMS/index.html. Publicly released records include, to name a few, NUREG-series publications; *Federal Register* notices; applicant, licensee, and vendor documents and correspondence; NRC correspondence and internal memoranda; bulletins and information notices; inspection and investigative reports; licensee event reports; and Commission papers and their attachments.

NRC publications in the NUREG series, NRC regulations, and *Title 10, Energy*, in the Code of *Federal Regulations* may also be purchased from one of these two sources.

1. The Superintendent of Documents
   U.S. Government Printing Office
   P. O. Box 37082
   Washington, DC 20402–9328
   www.access.gpo.gov/su_docs
   202–512–1800
2. The National Technical Information Service
   Springfield, VA 22161–0002
   www.ntis.gov
   1–800–553–6847 or, locally, 703–605–6000

A single copy of each NRC draft report for comment is available free, to the extent of supply, upon written request as follows:

Address: Office of the Chief Information Officer,
Reproduction and Distribution
Services Section
U.S. Nuclear Regulatory Commission
Washington, DC 20555-0001
E-mail: DISTRIBUTION@nrc.gov
Facsimile: 301–415–2289

Some publications in the NUREG series that are posted at NRC's Web site address www.nrc.gov/NRC/NUREGS/indexnum.html are updated regularly and may differ from the last printed version.

Non-NRC Reference Material

Documents available from public and special technical libraries include all open literature items, such as books, journal articles, and transactions, *Federal Register* notices, Federal and State legislation, and congressional reports. Such documents as theses, dissertations, foreign reports and translations, and non-NRC conference proceedings may be purchased from their sponsoring organization.

Copies of industry codes and standards used in a substantive manner in the NRC regulatory process are maintained at—

The NRC Technical Library
Two White Flint North
11545 Rockville Pike
Rockville, MD 20852–2738

These standards are available in the library for reference use by the public. Codes and standards are usually copyrighted and may be purchased from the originating organization or, if they are American National Standards, from—

American National Standards Institute
11 West 42nd Street
New York, NY 10036–8002
www.ansi.org
212–642–4900

The NUREG series comprises (1) technical and administrative reports and books prepared by the staff (NUREG–XXXX) or agency contractors (NUREG/CR–XXXX), (2) proceedings of conferences (NUREG/CP–XXXX), (3) reports resulting from international agreements (NUREG/IA–XXXX), (4) brochures (NUREG/BR–XXXX), and (5) compilations of legal decisions and orders of the Commission and Atomic and Safety Licensing Boards and of Directors' decisions under Section 2.206 of NRC's regulations (NUREG–0750).

NUREG-1726

Predictions of Spent Fuel Heatup After a Complete Loss of Spent Fuel Pool Coolant

Manuscript Completed: June 2000
Date Published: June 2000

Prepared by
C.F. Boyd

Division of Systems Analysis and Regulatory Effectiveness
Office of Nuclear Regulatory Research
U.S. Nuclear Regulatory Commission
Washington, DC 20555-0001

ABSTRACT

This generic study was done to predict the peak fuel temperatures and flow patterns observed after a complete loss of spent fuel pool coolant. The pool is assumed to be housed in a large containment building with an operable ventilation path. Fuel temperatures and natural circulation phenomena are predicted using computational fluid dynamics (CFD). These predictions identify the peak temperatures and the principal flow paths and features of the natural convective cooling phenomena for the coupled system of the fuel pool and containment building. The model is sized to represent a typical BWR pool and containment building. The pool is filled to its capacity with 4200 fuel bundles of various ages in high-density racking. Predictions are made with fuel loads representative of a fuel pool 2, 3, 4, and 6 years after the reactor is shut down. Sensitivity studies are done on the ventilation rate, the outer wall heat transfer coefficient, the location of the hottest fuel, fuel burnup, the flow resistance within the racks, and heat conduction within the racks. Best estimate predictions of critical decay time show that fuel temperatures remain below the temperature limits of 800 °C and 600 °C after 26 and 35 months of decay time, respectively. Predictions are made using the FLUENT CFD code. The finite volume mesh used for this model provides the resolution needed to resolve the important phenomena while remaining small enough to provide solutions with the available computer equipment. The overall size and computational complexity of the completed model preclude a rigid grid independence study. In considering quantitative results, the limitations and modeling assumptions must be kept in mind.

CONTENTS

FIGURES

TABLES

1 INTRODUCTION

In support of the Nuclear Regulatory Commission (NRC) rulemaking activity related to decommissioning, the office of Nuclear Reactor Regulation (NRR) is completing a study on spent fuel pool accident risks. In support, the Office of Nuclear Regulatory Research (RES) is providing technical assistance in several areas. This report documents a thermal-hydraulic evaluation of spent fuel pool heatup after a low-probability complete loss of spent fuel coolant. Computational fluid dynamics (CFD) is used to predict fuel heatup and natural circulation flow paths throughout the spent fuel pool and the upper containment building. The predictions give insights into the phenomena of air cooling which provides most of the heat removal capacity during long-term cooling scenarios after a complete loss of coolant.

Spent fuel pool heatup predictions are typically made using codes tailored to the geometry and physics of spent fuel stored in a rack. Codes of this type include SHARP[1], SFUEL, and COBRA-SFS. The SHARP manual (Ref. 1) provides general background information on some of the important phenomena considered in this type of model. A typical modeling approach is to determine one-dimensional buoyancy-driven flows between idealized upper and lower control volumes tying the fuel bundles together. Codes such as COBRA-SFS and SFUEL incorporate physical models for conduction, radiation, flow losses, clad oxidation chemistry, and other things. The flowfield assumptions, however, simplify the natural circulation flow paths in and around the fuel racks. The assumption of a single well-mixed volume joining each of the bundles at the top and bottom of the racks does not account for pressure or temperature variations in this region. The idealized upper control volume provides the ultimate heat sink for these models, simulating the entire building and the ventilation system.

Previous studies indicate that in steady-state conditions, the heat produced by the fuel is removed primarily through natural convection flows[2] (Ref 2, p. 47). In addition, the largest source of uncertainty in these fuel heatup predictions is the natural circulation flow rate[3] (Ref 3, p. 57). The RES predictions highlight the natural circulation flows that are simplified in typical spent fuel pool models. The focus of the predictions is on the three-dimensional natural circulation flowfield in and around the fuel pool, racks, and containment building. Physical models for radiation and clad chemistry are not incorporated. The predictions can be used to assess the flowfield assumptions used in other codes. The three-dimensional CFD predictions made by RES give valuable insights into the natural circulation air flow which is crucial to spent fuel pool cooling after a complete loss of spent fuel pool coolant.

All code results must be viewed in the light of the assumptions used for the analysis. The CFD model makes simplifying assumptions to represent the complex geometry of the racks and fuel. A porous region provides an equivalent flow resistance for the rack and bundles and aligns the flow in the vertical direction. A volumetric heat source adds the appropriate energy to the fluid in the active fuel region. Predictions are obtained for steady-state conditions to determine the maximum fuel surface temperature for a given pool age and configuration. The CFD predictions do not include models for radiation and clad chemistry. These models are considered important at elevated temperatures ($T > 600$ °C, Ref 2, Figs. 12, 14 and 26). Therefore, the current CFD predictions are more applicable at low temperatures, where these effects are minimal. At elevated temperatures, potential limitations should be kept in mind.

2 COMPUTATIONAL FLUID DYNAMICS (CFD)

The FLUENT[4] (version 5) CFD code is used to predict the temperature rise in the fuel and the natural circulation flow rates. FLUENT is a commercially available, general-purpose CFD code capable of solving a wide variety of fluid flow and heat transfer problems. The code solves the Reynolds-averaged Navier-Stokes equations a finite volume mesh. The Navier-Stokes equations are the mass, momentum, and energy equations for a continuous fluid. Reynolds-averaging creates the need for turbulence modeling to account for the turbulent diffusion of momentum and energy. The FLUENT code provides several turbulence modeling options and can be applied to almost any geometry.

The predicted results from a CFD analysis are influenced by several steps in the process. In a blind study, where no experimental data are used for bench marking the code, the analyst must rely on accepted CFD practices and engineering judgment to create an acceptable CFD simulation. The basic steps of a CFD analysis are to describe the physical model, develop the CFD model, do sensitivity studies, and validate the solution. Commercial CFD codes are widely used in many industries today. The fundamentals of CFD are to be found in textbooks such as the introductory text by Anderson[5].

3 PHYSICAL MODEL DESCRIPTION

A simplified model of the containment building, fuel pool, racks, and ventilation system is developed for this investigation. The major parameters used and the physical features of the pool are determined with input from the Office of Nuclear Reactor Regulation (NRR). The model is based upon a boiling water reactor (BWR) containment and fuel pool. The major components are described below.

3.1 Pool and Racks

The pool and fuel rack dimensions are typical of a large BWR. The pool is assumed to be completely filled with high-density racking. The racks extend to within 0.15 m (6 in.) of the fuel pool walls. To establish symmetry, the pool is centered on the long axis of the containment building. Figure 1 shows the features of the fuel pool cut along the line of symmetry. The finite volume cells used to represent the rack region in the CFD model are included to highlight the location of the racks. Overall pool dimensions are 9.54 m x 11.08 m x 12 m (l, w, d). The fuel racks sit 0.15 m (5.9 in.) from the pool floor and are 4.3 m (14.1 ft) in height. The high-density racking occupies the entire lower pool (except the 0.15 m gap around the exterior). Figure 2 shows the structure of a typical high-density rack. The square cells which make up the rack share a wall between neighboring cells and there are no open cells. The walls are solid so there is no communication of fluid between cells. Cell pitch is 0.154 m (6 in.). Rack-to-rack spacing is ignored in this model, which is equivalent to assuming a single rack structure with 4200 cells (60 x 70; 9.24 m x 10.78 m). Assuming a full core contains 800 bundles, this pool is racked to hold 5 ¼ cores.

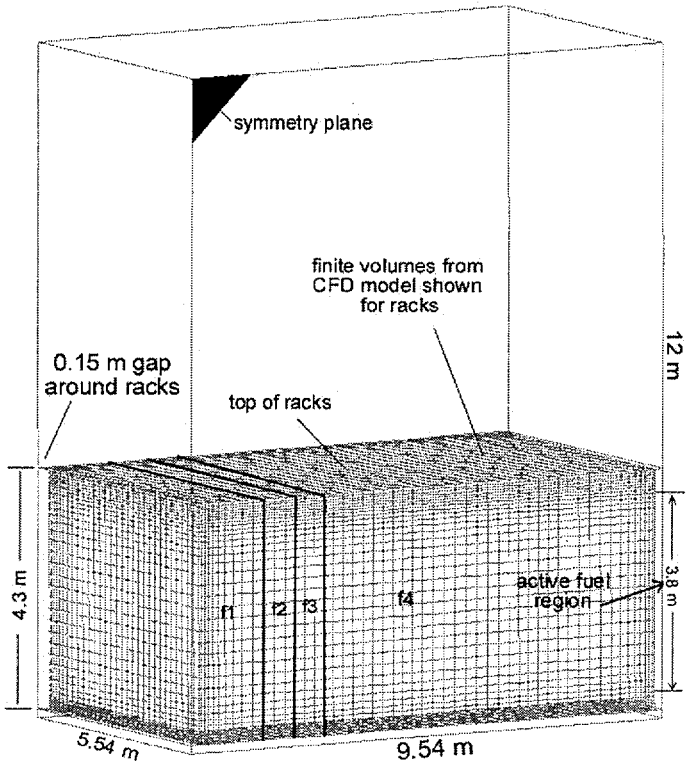

Figure 1. Pool Region and Racks

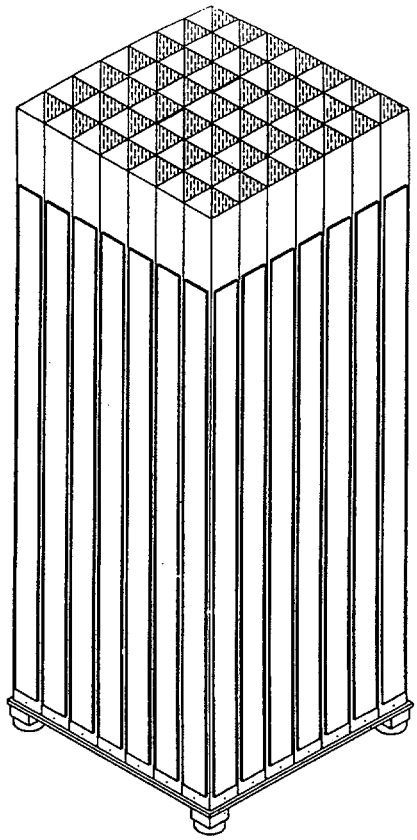

Figure 2. High-Density Fuel Rack

3.2 Fuel

A fuel bundle is assumed to occupy each cell of the high-density racking (4200 assemblies). A uniform active (heat generating) length of 3.8 m (12.46 ft) is centered from top to bottom in the racks. Four pool regions are defined with unique characteristics. A hot region with 800 bundles (f1 = 1 core), a second region with 267 bundles (f2 = 1/3 core), a third region with 267 bundles (f3), and a final region with 2866 bundles (f4). Fuel f2 is assumed to be 18 months older than fuel f1 and fuel f3 is 18 months older than fuel f2. Region f4 represents all of the remaining (older) fuel. The fuel layout is illustrated in Figure 1. The hot fuel (f1) is assumed to remain in a contiguous region on the left side of the pool. Fuel f2 is in another contiguous region next to the hottest fuel. Next comes fuel f3. The remaining 2866 bundles, f4, fill out the rack. A sensitivity study is done to look at the effect of moving the hottest fuel, f1, to the center of the pool. More details on the geometry of the 9 x 9 bundles are given in Appendix A, "Flow Loss Coefficients through BWR Fuel Storage Racks." Table 1 lists the fuel loads applied in this analysis. The fuel loads are given in watts per bundle. These loads are based upon an average burnup of 40 or 50 GWd/MTU, as noted. Most of the predictions assume an average burnup of 40 GWd/MTU for each fuel region. A sensitivity study is done assuming a burnup of 50 GWd/MTU.

Table 1. Fuel Loads for Whole Pool

	No. of cores	No. of cells	Average Watts/bundle after number of years				
			2 yr (40)*	3 yr (40)*	4 yr (40)*	4yr (50)*	6 yr (40)*
f1, Hot	1	800	920	620	462	576	341
f2, Med Hot	.33	267	536	419	360	457	296
f3, Med Cold	.33	267	381	341	304	390	272
f4, Cold	3.6	2866	201	198	194	246	190
Total heat load (megawatts) >>>			1.557	1.266	1.103	1.392	0.969

* Average Burnup (GWd/MTU)

3.3 Containment Building

The main building is sized to represent a BWR containment. No internal structures are modeled. The size and location of the containment relative to the fuel pool is shown in Figure 3. This figure represents the CFD model domain, which is a symmetrical half of the physical structure. The plane of symmetry faces out toward the reader. The containment building is modeled only from the pool surface up to the ceiling. Lower levels are ignored.

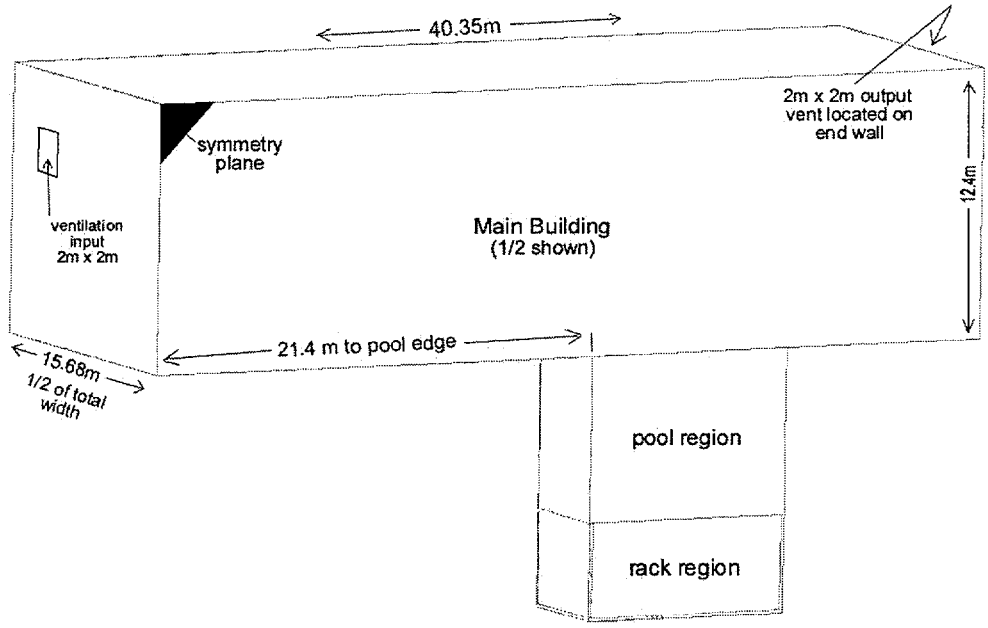

Figure 3. Containment Building With Fuel Pool

3.4 Ventilation

A single ventilation input and output are used in the CFD model, which represents half the building and fuel pool. The ventilation opening is 4 m^2 and is shown in Figure 3. The standard ventilation rate is based upon 2 building volumes of air exchanged per hour (Ref. 2, p. 41). The inlet flow provides 2 building volumes of air to the building every hour. Sensitivity studies are performed on this value. Air enters the containment through the inlet vent and is heated by the fuel. Inlet air is set at 27 °C. Air is exhausted on the opposite end of the building through a similar vent opened to the atmosphere. The inlet and outlet vents are positioned 2.68 m from the back wall and ceiling of the containment building.

3.5 Wall Heat Transfer

Most of the predictions assume the external building walls are adiabatic. Sensitivity studies are done on the overall heat transfer coefficient at the side walls and ceiling of the containment building. Values of 0, 2, and 4 W/m^2-K are used. Best estimate values range[6] from 1 to 3 W/m^2-K. This range covers various wall types subjected to a 15 mph outdoor wind speed. Outdoor air is assumed to be 27 °C. A value of 2 W/m^2-K is used for best estimate predictions in this report. The pool walls and containment floor are always modeled as adiabatic.

4 CFD MODEL DEVELOPMENT

The physical model described above is represented on a set of finite volumes on which the governing equations are discretized and solved. The Reynolds-averaged Navier-Stokes equations are used. Boundary conditions are applied on the model to facilitate a solution. Developing a CFD model requires a balance between the size and complexity of the model and the need to obtain solutions within available time and computational resources. Although the computational resources available to RES are significant, the scale of this problem dictates that simplifications must be made. The assumptions used to develop the CFD model are discussed below. The model is for use in the FLUENT version 5 unstructured CFD code.

Each prediction is run to find a steady-state solution, using typical CFD modeling options. The solutions give the maximum expected temperature but not the time it takes to reach it. A transient analysis would require significantly more computer time. The major features of the CFD model are given below.

- steady state Reynolds averaged Navier-Stokes solution
- k-epsilon turbulence model with standard wall functions
- ideal gas, variable thermal properties (air as working fluid)
- gravity
- 675,000+ finite volume cells (tetrahedron and hexagonal mesh)
- segregated solver with 2nd order differencing on momentum and energy
- porous media model of fuel and racks (vertical laminar flow through region)

The clad oxidation reaction and radiative heat transfer are not included in this model. The effect of these omissions is considered small at temperatures below 600 °C. Higher temperature results should be considered with this limitation in mind. These effects may be studied in the future using the FLUENT code.

4.1 Finite Volume Mesh

The mesh consists of over 675,000 finite volumes (Figure 4). The mesh design minimizes the number of cells used for the model while providing an adequate number of cells to resolve important physical gradients. Cells are constructed to have minimal skew and sides of equal length (aspect ratio = 1) wherever possible. Cell to cell growth is limited to a range between 0 % and 20 %.

Cells in the upper building are large, 1 m^3, to save resources, so excess diffusion is expected in this region. This concession is not considered serious. Flows in the upper building are expected to be more complex (more diffusive) in the typical containment due to internal structures omitted in the CFD model. Any numerical diffusion resulting from the large cells in the upper building will enhance mixing, which is expected to be underpredicted by this model.

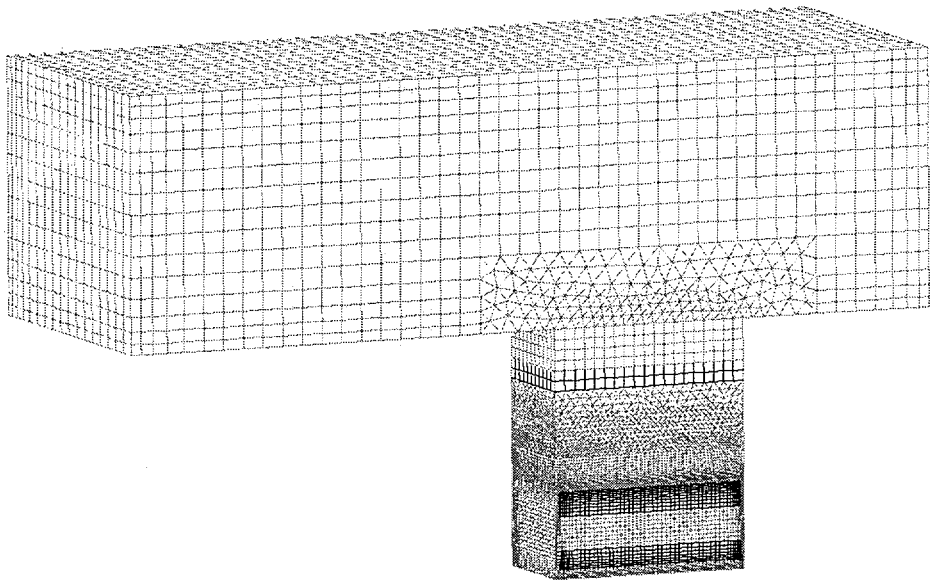

Figure 4. Finite Volume Mesh for CFD Predictions

Most of the 675,000 cells are located in and around the fuel racks where the highest gradients and most significant phenomena occur. Cell height at the top of the racks is reduced to 1 cm through the use of grid adaption. This fine resolution is needed to resolve the large thermal and velocity gradients predicted in this region. Transitions from the very fine mesh to regions with larger mesh are constructed of tetrahedral elements with a controlled growth rate. This technique eliminates the skew in the hexagonal element regions and provides a smooth transition between cells of different sizes.

4.2 Boundary Conditions

Boundary conditions are applied at the walls (both internal and external) and at the inlets and outlets. All external walls use the no-slip condition for the momentum equations. No surface roughness is applied. All external walls are adiabatic except as noted in the sensitivity studies.

The surface facing the reader in Figure 4 is a symmetry plane. Internal vertical walls are positioned within the fuel and rack region to separate zones of different fuel ages and to align the flow vertically. These internal walls use a no-shear boundary condition since all flow resistance within the racks and fuel is accounted for by the porous model.

Fresh air enters the building through the 4 m^2 inlet vent (Figure 3). At this location, the flow is aligned normal to the building wall and has a turbulence level of 10%. The inlet velocity is set to yield a volume flow rate equivalent to 2 building volumes per hour (except as noted in sensitivity studies). The input air is 27 °C. The prescribed inlet velocity is 1.1 m/s. Air exits the model at the opposite end of the building. The exit vent is modeled as a pressure boundary set to atmospheric conditions (101325 Pa, 27 °C).

4.3 Material Properties

The working fluid is air modeled as an ideal gas. The temperature-dependent thermal properties are given in Table 2. These properties are obtained from White's *Viscous Fluid Flow*[7]. The FLUENT code uses linear interpolation between points in the material property tables. For temperatures above the maximum tabulated value (1000 °C), the FLUENT code uses the thermal properties associated with the maximum value in the table. This assumption is valid as long as the temperatures do not go significantly above the values in the table.

Table 2. Material Properties, Air (White, 1988)

Temperature °C	Cp (J/kg-K)	k (W/m-K)	viscosity (Pa-s)
0	1003	.0242	1.72 e-05
100	1010	.031	2.17 e-05
200	1024	.0376	2.57 e-05
300	1045	.0439	2.93 e-05
400	1069	.0497	3.25 e-05
500	1093	.0553	3.55 e-05
600	1114	.0609	3.83 e-05
700	1135	.0659	4.09 e-05
800	1153	.0703	4.34 e-05
900	1170	.0747	4.57 e-05
1000	1184	.0786	4.79 e-05

4.4 Fuel and Racks

The fuel and rack structure are not modeled in detail; the geometry of this region is too complex. CFD modeling of the details of every bundle in a fuel pool is impractical because of memory and processor limitations. To simplify the model, a homogenous nonisotropic porous medium is used to represent the racks and fuel. The volume occupied by the racks is replaced by the porous medium designed to affect the flowfield as the rack structure and fuel would. A porous material does not affect the flow area in the FLUENT model. Flow resistance is set through user-defined viscous and inertial flow loss coefficients. Details of the resistance coefficient determination are given in Appendix A. Lateral flow resistance in the porous medium is set two orders of magnitude higher than the vertical resistance to ensure vertical flow through the racks. Several vertical internal walls are also included in the racks to further guarantee a vertical flow path. The fuel is centered vertically in the racks and has a uniform active heated length of 3.8 m. The width of the active fuel region is 9.24 m, as shown in Figure 1. The individual fuel widths are defined to keep the fuel proportions the same as in Table 1. Fuel regions f1 to f4 are 1.76, 0.5874, 0.5874, and 6.3052 m wide, respectively. Heat is added to the flow as a uniform volumetric heat generation term throughout the volume occupied by the fuel. Axial heating distributions are not considered. Radiation and clad chemistry are not included in the model.

Thermal inertia and thermal conduction within the fuel and racks are accounted for in the FLUENT model through the porous media options. The material properties of the medium and the porosity of this region are prescribed to account for the thermal inertia of the racks and fuel and to approximate axial thermal conduction. The FLUENT porous media model assumes isotropic conductivity so the single value affects axial and lateral conduction. A sensitivity study on the thermal conductivity is done to give further insights into the significance of this parameter. Details of the porous media assumptions used to account for thermal inertia and thermal conductivity in the rack region are given in Appendix B.

4.5 Turbulence Modeling

The k-epsilon turbulence model is used for this analysis with standard wall functions. This model is selected because of its robustness and ease of application. It is acknowledged that the k-epsilon turbulence model is not tailored to this type of problem. Experimental data are needed to refine the turbulence modeling beyond this standard approach. This subject is beyond the scope of this initial study.

The flow up (or down) through the bundles is expected to be laminar because of the low Reynolds number in this region. For example, if the velocity of 400 °C air is .243 m/s along the tube bundles (0.1 m/s in the open porous region of the FLUENT model), the Reynolds number based upon hydraulic diameter would be close to 50, indicating laminar flow. To account for this laminar flow, the porous media region representing the racks and fuel is modeled as a laminar region. In this region, turbulence production and turbulent viscosity are disabled. The FLUENT code model transports the turbulent properties through the region unchanged.

4.6 Solution Convergence

Final results from this analysis are somewhat unsteady. Variations of +/- 20 °C in the hottest fuel temperatures are typical. To obtain final results, the model is executed until the oscillations are in a steady-state pattern. At this point, variables are recorded during one or more oscillations and an average value is recorded. Initial convergence of the solution is monitored by observing temperatures and velocities at various points in the domain as a function of time. In addition, the residuals (a measure of error) are monitored and minimized for each solution. As a final check, the overall mass and energy balances are verified.

4.7 Grid Independence

A grid independence study is not feasible due to the physical scale of the model and the limited computer resources. A high quality mesh is used for this analysis to minimize any grid affects on the results. The effect of the assumptions on the final solution are expected to far outweigh any small effect of the grid on the predictions. Qualitative information on grid independence is given below for completeness.

The final grid for this study contains over 675,000 finite volume cells. In the process of constructing this grid, over 10 separate grids are created and tested. The final grid is a compilation of the lessons learned during this process. The lessons learned included node density requirements for wall functions and large gradients. The final mesh is created with as many cubical elements as possible. Grid stretching and skew are minimized. Mesh size is reduced at the walls to accommodate the wall functions and transitions away from the wall are limited to growth rates between 5% and 20%. To transition between nearly cubical elements of different scales, tetrahedral regions are constructed with growth rates between 5% and 20%. The largest gradients are found just above the fuel racks. In this region, grid adaption is used twice to reduce the grid size to approximately 0.01 m. Unphysical results were observed in some of the earlier models without this adaption. Grid adaption is also used to refine the mesh in the open region around and below the racks.

5 COMPLETED PREDICTIONS

CFD results are most valuable when a series of predictions are made with varying assumptions and inputs to assess their impact on the predicted results. This is especially true when there is a lack of data available for model validation. Sensitivities of the final predictions to changes in assumptions and parameters gives valuable insights into the predictions. Table 3 gives the major parameters and assumptions varied for each prediction. As noted in Table 3, several sensitivity studies are completed which include variations of the following parameters:

- decay time
- ventilation rate
- flow resistance within the fuel and racks
- heat transfer coefficient for external building walls
- fuel loading pattern (location of hottest fuel)
- porous media thermal conductivity
- fuel burnup

Table 3. Completed Predictions

	Decay time (yrs)	Fuel burnup (GWd/ MTU)	Vent (bldg./ hr)	Overall h (W/m^2-K)	Sensitivity study notes
f2v2h0	2	40	2	0	2 yr, adiabatic walls
f3v2h0	3	40	2	0	3 yr, adiabatic walls
f4v2h0	4	40	2	0	4 yr, adiabatic walls (base case)
f6v2h0	6	40	2	0	6 yr, adiabatic walls
f4v1h0	4	40	1	0	vent 1 building per hour
f4v1p5h0	4	40	1.5	0	vent 1½ buildings per hour
f4v2p5h0	4	40	2.5	0	vent 2½ building per hour
f4v2h2	4	40	2	2	wall heat transfer (h = 2 W/m^2-K)
f4v2h4	4	40	2	4	wall heat transfer (h = 4 W/m^2-K)
f4v2h0rp	4	40	2	0	rack/fuel flow resistance +20%
f4v2h0rm	4	40	2	0	rack/fuel flow resistance -20%
f4mv2h0	4	40	2	0	hottest fuel in center of pool
f4v2h0km20	4	40	2	0	porous conductivity -20%
f4v2h0km50	4	40	2	0	porous conductivity -50%
f4v2h0b50	4	50	2	0	fuel burnup = 50 GWd/MTU
f2v2h2	2	40	2	2	2 yr best estimate, (h = 2 W/m^2-K)
f3v2h2	3	40	2	2	3 yr best estimate, (h = 2 W/m^2-K)
f6v2h2	6	40	2	2	6 yr best estimate, (h = 2 W/m^2-K)

The 4 year case, f4v2h0, is used as the base case. Most sensitivity studies begin with or pass through f4v2h0. Best estimate results use a wall heat transfer coefficient of 2 W/m^2-K.

6 SUMMARY OF ASSUMPTIONS AND LIMITATIONS

The completed CFD predictions give valuable insights into the three-dimensional natural circulation air flows. These flows provide the primary heat removal mechanism in a postulated complete loss of spent fuel pool coolant accident. The final results, however, are still dependent upon the modeling assumptions and limitations. To ensure that these issues are considered along with the final results, some major assumptions and limitations are listed in Table 4.

Table 4. Assumptions and Limitations

Assumptions	Notes/Limitations
building and pool dimensions	building and pool are within typical range but do not represent all configurations
4200 fuel assemblies, high density racks	no rack-to-rack spacing, no open areas in pool
flow resistance in rack/fuel region	determined from a typical configuration, does not apply to all rack designs
0.15 m (6 in.) gap from rack to pool wall	typical for a full pool; some gaps reported as small as 0.05 m (2 in.)
no structures within building	plant-specific structures could affect the flow
model pool and containment above pool surface level	containment only modeled from pool surface up, plant-specific features could affect solution
2 buildings per hour ventilation rate	typical of an operable ventilation system, location of vents could affect the flow patterns
fuel arranged in contiguous regions by age	no checker boarding of fuel is attempted, no open cells are in racks
decay heat levels	average value used for each fuel grouping, best estimate for expected high burnup fuel
porous media	rack structure is homogenized, heat is added directly to the flow, fuel surface is not modeled, flow resistance is modeled, isotropic conduction
external pool walls are adiabatic	only heat transfer from upper building and ceiling is considered
uniform heat generation in fuel	axial fuel peaking is ignored
radiation	neglected, can be important at elevated T
clad oxidation reaction	neglected, can be important at elevated T
steady-state solution sought	no transient information available during heatup
CFD modeling assumptions and grid	no data used for assessing turbulence modeling, grid independence is not verified

7 RESULTS

The base case, f4v2h0, is described in detail to illustrate the flow phenomena predicted and to define some of the parameters used to describe the results. Next, the results for each of the predictions are summarized in tables. Finally, the sensitivity study results are summarized.

7.1 Base Case Results (f4v2h0)

The base case uses a 4 year decay time with the hottest fuel located along the left edge of the pool. All external walls are adiabatic. The ventilation rate is based upon two building volumes per hour, which corresponds to an inlet air velocity of 1.1 m/s. The inlet air temperature is 27 °C and the flow has a 10% turbulence level at the inlet. The inlet vent flow area is 4 m^2. Important parameters and phenomena predicted for this case are described below.

7.1.1 Maximum Temperature

The maximum temperature predicted during this scenario varies with time. The peak temperature predicted is 540 °C with variations of +/- 20 °C. Peak temperature is observed near the top of the hottest fuel and on the symmetry plane. Figure 5 shows the computational domain with temperature contours displayed on the surface of the active fuel region. The hottest regions are lightest (whitest) in the figure.

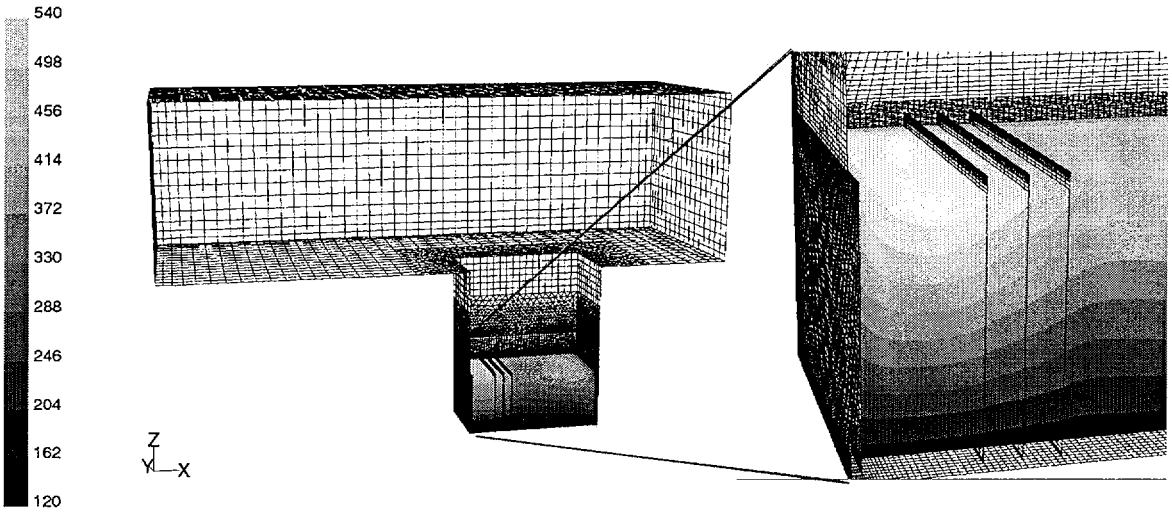

Figure 5. Temperature Contours on Active Fuel Region

Walls between the fuel types are left in place as a visual aid. There is an additional vertical wall in fuel region f1 and several additional walls in fuel region f4. To clarify the image, these walls are omitted. The hottest fuel, f1, is on the left, with a temperature approaching 540 °C. The air entering the bottom of the hottest fuel is approximately 125 °C. Actual fuel surface temperatures can be approximated using Newton's law of cooling. The Nusselt (Nu) number is approximately[8] 9. The difference between the predicted air temperature (assumed to be the mixed mean) and the surface temperature is predicted to be less than 10 °C. This difference is considered negligible and the maximum temperatures are therefore simply reported as the maximum predicted air temperatures.

7.1.2 Global Flow Pattern

The overall flow, although unsteady, displays a predictable pattern. Figures 6, 7, and 8 illustrate the principal convective flow paths. Figure 6 shows the volume of air that is predicted to have temperatures in the range of 132 to 500 °C. These limits are chosen to highlight the hot plume of air rising from the side of the pool containing the hottest fuel. The rising plume stays near the left pool wall until it enters the main building. At this point, the hot air flows towards the roof of the containment with a slight preference for the outlet vent. The rising hot air hits the ceiling and spreads to cover the entire ceiling with a layer of hot air. Although the air temperature peaks at over 500 °C in the fuel racks, the rising plume of hot air cools rapidly as it rises. The maximum temperature is 200 °C just a few meters above the fuel racks. As the hot plume reaches the top of the pool, the maximum temperature is 160 °C. The maximum plume temperature is 135 °C when the plume hits the ceiling. Temperatures in the containment are predicted to stratify significantly. The temperature of the hot air on a horizontal plane 0.5 m below the ceiling ranges from 130 to 135 °C. Eliminating the small region occupied by the plume reduces the temperature variation on this horizontal plane to less than 2 °C.

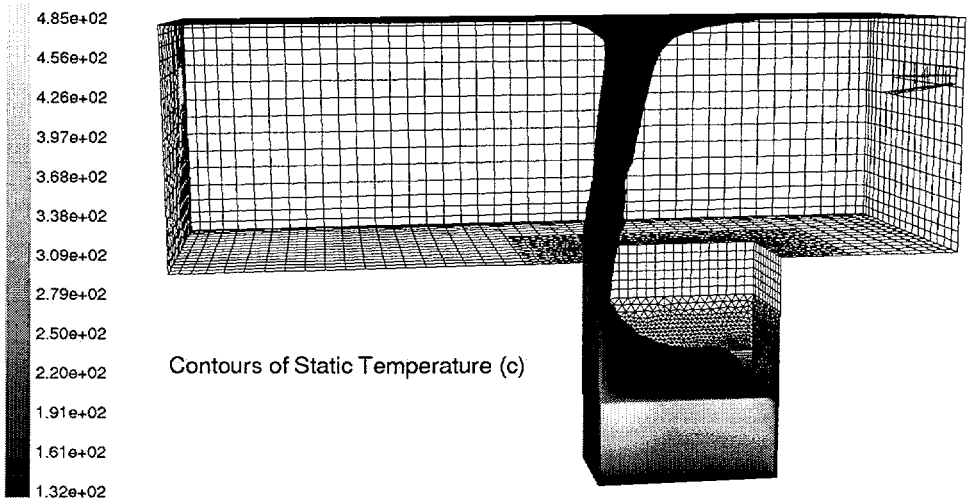

Figure 6. Temperature Contours Showing Rising Hot Plume

Figure 7 shows the inlet air entering the containment and falling to the floor of the building. This relatively cool air spreads around the rising hot plume exiting the pool and falls into the pool on the opposite side. The air on the floor of the containment is relatively well mixed. The temperature range observed on a horizontal plane 0.5 m above the containment floor is 80 to 160 °C. Eliminating the small regions where the inlet plume first hits the floor and where the hot plume rises through this plane results in a temperature range at this elevation of 90 to 110 °C. The average temperature difference between the floor and the ceiling in the containment is approximately 30 °C.

A detailed view of the flowfield just above the containment floor is given in Figure 8. This figure shows the velocity vectors on a plane 0.5 m above the floor. The cold inlet plume is predicted to hit the floor and spread out in all directions. The flow travels across the containment floor

and around the rising plume. The flow falling into the pool is also clearly visible. The pool edges are not visible. The increase in vector density in the rectangular region around the pool is the result of a mesh density variation near the pool. The mesh density variation and the pool edges are visible in Figure 6. The cold air that enters the fuel pool hits the top of the racks (like a stagnation point) and then flows outward towards the pool walls. Most of the cooling air travels down around the racks (along walls) to the floor of the fuel pool and then up through the fuel.

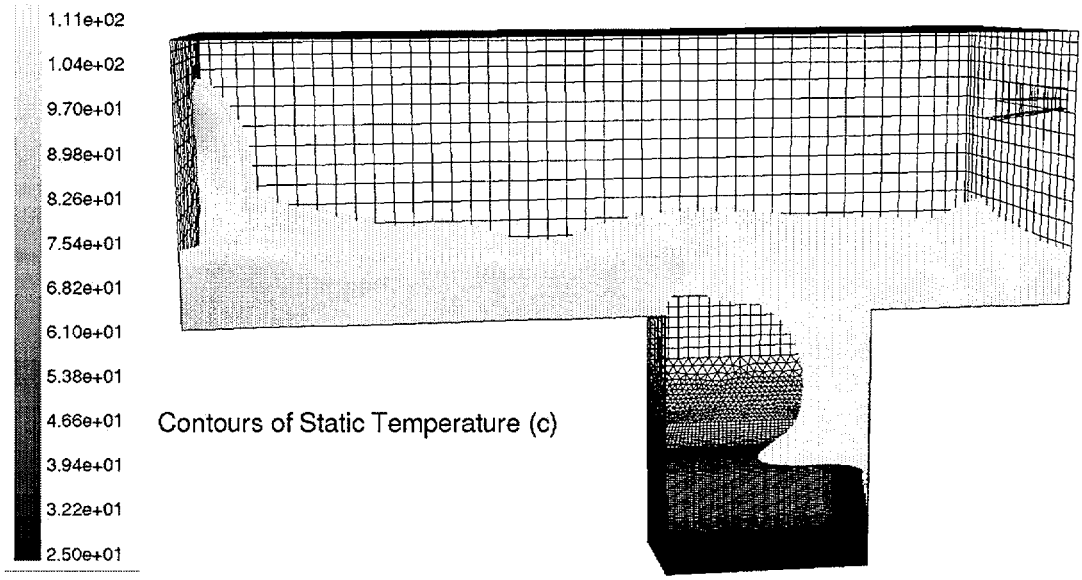

Figure 7. Temperature Contours Showing Cooling Air Flow

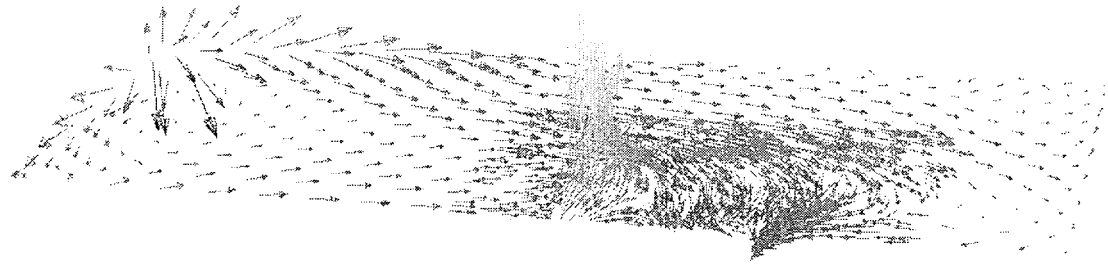

Figure 8. Velocity Vectors in a Plane 0.5 m Above the Containment Floor

7.1.3 Global Energy Balance

To verify a global energy balance, the first law of thermodynamics is applied to the system using a control volume approach. The outlet temperature is computed and compared to the prediction from the FLUENT code. The relevant energy terms are the energy input from the fuel, the energy lost at the external walls by convection, and the energy transported away by the ventilation system. In this case, all the heat generated by the fuel is carried away by the natural circulation flows since the walls are adiabatic. The first law of thermodynamics applied to this steady-state/steady-flow problem results in the following balance of energy equation:

$$\dot{Q}_{fuel} - \dot{Q}_{walls} + \dot{m}(h_{inlet} - h_{outlet}) = 0$$

The terms in the equation represent the energy from the fuel, the energy lost at the walls due to convection, and the net energy change between the inlet and the outlet flows. For this case, total heat from the fuel, Q_{fuel}, is 551,474 W. The wall heat transfer, Q_{wall}, is 0. Assuming 26.85 °C air entering the building through a 4 m^2 inlet vent at 1.10 m/s results in an inlet mass flow rate of 5.178 kg/s. From thermodynamic tables, the inlet enthalpy (h_{inlet}) is 300.19 kJ/kg. Using these values for the total heat load, the mass flow rate, and the inlet enthalpy, the energy balance predicts an outlet enthalpy (h_{outlet}) of 406.69 kJ/kg. From thermodynamic tables, this translates into an outlet temperature of 132.5 °C. The predicted outlet temperature from FLUENT is 132.7 +/- 5 °C. The FLUENT code maintains a global energy balance.

7.1.4 Flow In and Around Racks and Fuel

The flow from the upper building enters the pool and falls to the racks as shown in Figure 7. The flow turns at the rack surface. Some of the flow is entrained by the rising hot air and exits the pool. Some travels down and around the fuel racks to the pool floor, where it spreads out to cover the region below the racks. As air is pulled up through the fuel and racks, it forms the hot plume visible in Figure 6. The regions of up and down flow in the rack region are illustrated in Figure 9. This figure shows contours of vertical velocity on a horizontal plane at the top of the active fuel region (z = 4.2 m).

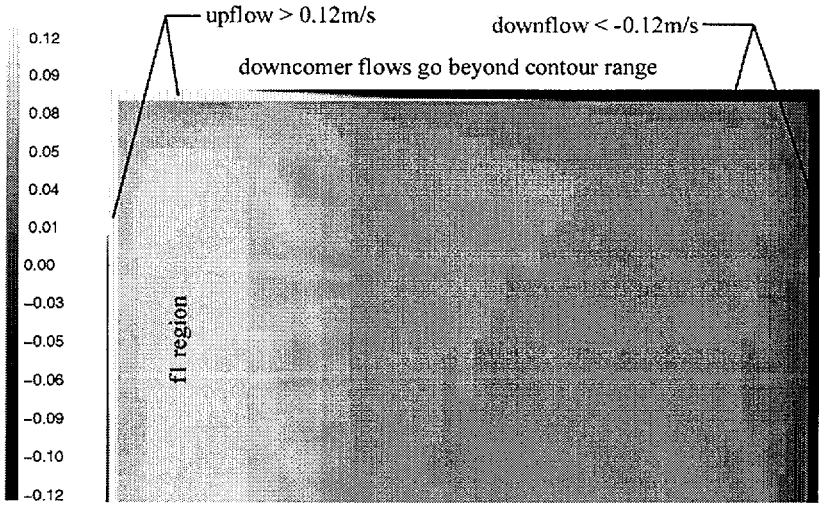

Figure 9. Vertical Velocity (m/s), Horizontal Plane, Top of Active Fuel

The contour ranges are limited to +/- 0.12 m/s to highlight variations in the fuel region. Downcomer velocity magnitudes go beyond these limits, however. Regions where the velocity is above or below the contour ranges are displayed with the maximum or minimum contour range. The velocity in the fuel is positive (upward) everywhere except a small region near the right downcomer.

A slight upflow is predicted for the left downcomer. This upward flow is the result of several factors. First, the strong plume formed by the hottest fuel blocks downflow on the left side of the pool. In addition, the left downcomer is subject to some buoyant forces due to heat transfer from the hottest fuel adjacent to this region. Entrainment of air in the rising plume on the left side of the pool also promotes upflow in the left downcomer. Finally, a strong right-to-left flow under the fuel racks feeds the flow up through this downcomer.

Most of the flow to cool the fuel enters the region below the racks from the downcomer on the right side of the pool. This region is supplied by a significant downflow of cooling air from the upper building. The air entering the region below the racks spreads across the floor, as shown in Figure 10. In this figure velocity vectors are shaded with temperature on a plane midway between the floor of the pool and the lower edge of the racks (z = 0.075 m). Figure 10 clearly shows that the source of cooling air is the right downcomer.

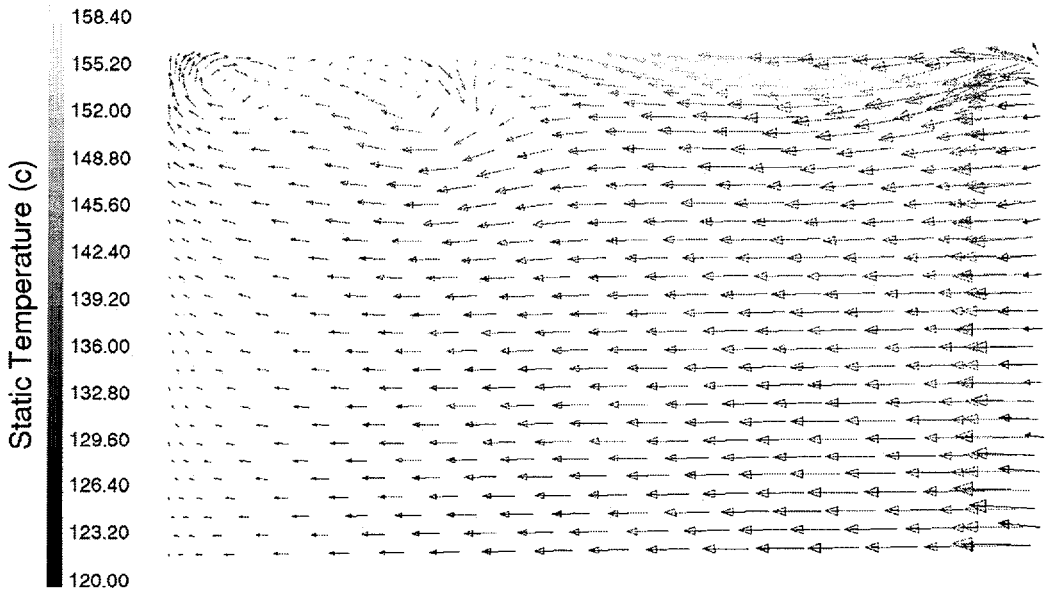

Figure 10. Velocity Vectors Shaded With Temperature Below the Fuel Racks

Flow in the third downcomer region (top of Figure 9) is more complex. No strong up or down flow is observed. The left side has a slight upflow and the right side has a slight downflow. Large recirculations are observed in this region, making it difficult to generalize the flow path. All fuel and downcomer flows are summarized by the net mass flow rate through each region. Mass flow rates are reported on a horizontal plane at the top of the active fuel region (z = 4.2 m), with positive values indicating upward flow.

Net mass flow through a horizontal plane at the top of the active fuel is given in Table 5 for the four fuel regions and three downcomer regions. The predicted mass flow rates are slightly unsteady. Reported values represent an average mass flow rate for a series of predicted values over time.

Table 5. Mass Flow Rates at Top of Active Fuel, Base Case

Region	Mass Flow Rate (+ upflow, kg/s)	Average Mass Flux (kg/m^2 s)
left downcomer	0.22	0.27
right downcomer	-1.58	-1.90
rear downcomer (top of Fig. 9)	-0.18	-0.13
net downcomer >>	**-1.54**	**-0.51**
f1	0.41	0.043
f2	0.13	0.041
f3	0.12	0.037
f4	0.89	0.018
net fuel >>	**1.54**	**0.031**

7.1.5 Pressure Above and Below Rack

Spatial pressure variations are predicted above and below the racks. These predictions can be used to assess the applicability of the constant pressure boundary condition used in other spent fuel pool models in these regions. All predictions are given as a gauge pressure referenced to the atmospheric pressure at the outlet vent.

Figure 11 shows the predicted pressure on a horizontal plane at an elevation of z = 4.5 m. This plane is 0.05 m (2 in.) above the top of the racks. Pressures vary from 15.25 to 18.25 Pascal (Pa). The average pressure at this elevation is 16.7 Pa. The right side of Figure 11 shows the highest pressure near the symmetry plane. Figure 7 shows why: the relatively cool air flows down the right side of the pool and impinges on the racks there. This region of high pressure is the result of the stagnation region created by the falling plume as it turns 90 degrees to flow along the top of the racks. The stagnation point is on the axis of symmetry near the right downcomer. Flow vectors radiate from this point in all directions as the velocity vectors, not shown, clearly demonstrate.

The magnitude of the pressure variation across the top of the racks is predicted to be approximately 3 Pa. This value is considered significant relative to the pressure differences encountered. For example, the predicted difference between the average

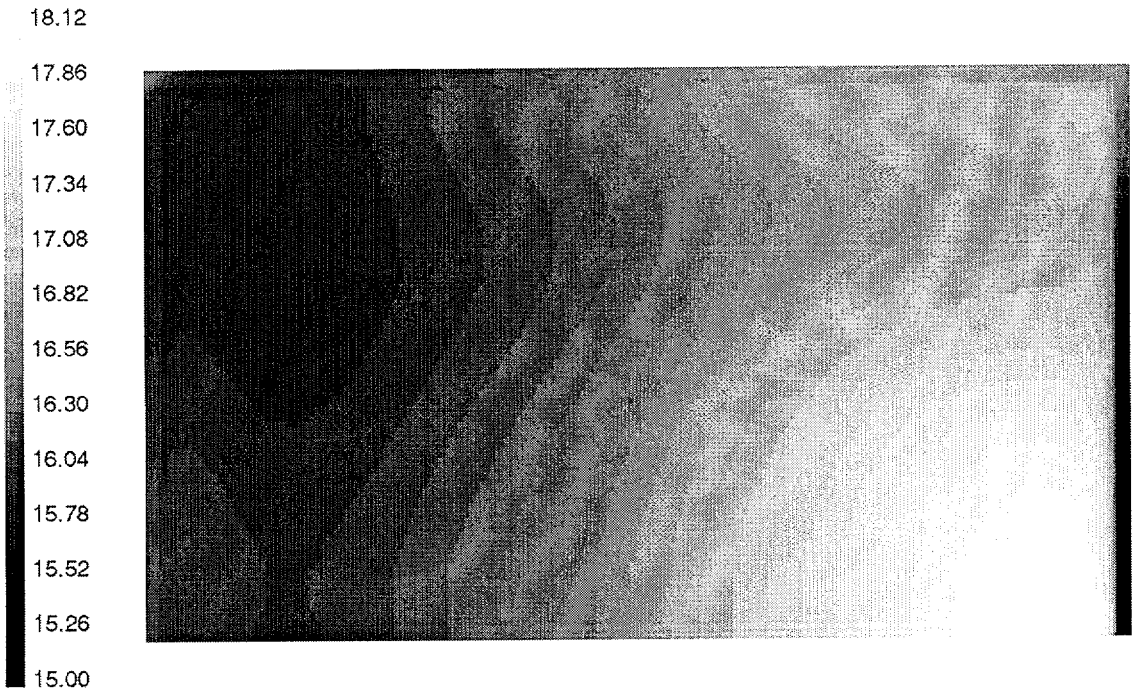

Figure 11. Pressure Contours Above the Fuel Racks, Pa (z = 4.5 m)

pressure above and below the racks for the base case is 5 Pa. Flow losses are also in this range. Consider air at 900 °C flowing through the racks and fuel at 0.1 m/s. The pressure drop (no gravity) is approximately 15 Pa based upon the coefficients in Appendix A. If the air is 400 °C and flowing at 0.01 m/s, the expected pressure drop is close to 1 Pa. Considering these pressure differences, the 3 Pa variation across the top of the racks could be significant.

Figure 12 shows the predicted pressure contours below the rack at an elevation of 0.1 m. This plane is 0.05 m from the bottom of the racks. Pressures vary from 7.25 to 15.25 Pa; the average pressure is 11.8 Pa. The right side of Figure 12 shows the highest pressure at the bottom of the right downcomer. This is the region where the strong downflow hits the floor and turns to flow along the bottom of the racks. The high velocities leaving this region result in low pressures to the left of the stagnation region. The static pressure slowly increases as the flow slows down on its way to the hottest fuel region at the left. As noted earlier, the reported pressure variations at this plane are significant with respect to other relevant pressure differences in this region.

7.1.6 Temperatures Above and Below Rack

The temperatures above and below the rack are given by Figures 13 and 14, respectively. These results are highlighted to provide a basis for assessing the constant temperature boundary condition assumed by some spent fuel codes. Temperatures are given on the same horizontal planes used to illustrate pressure in Figures 11 and 12.

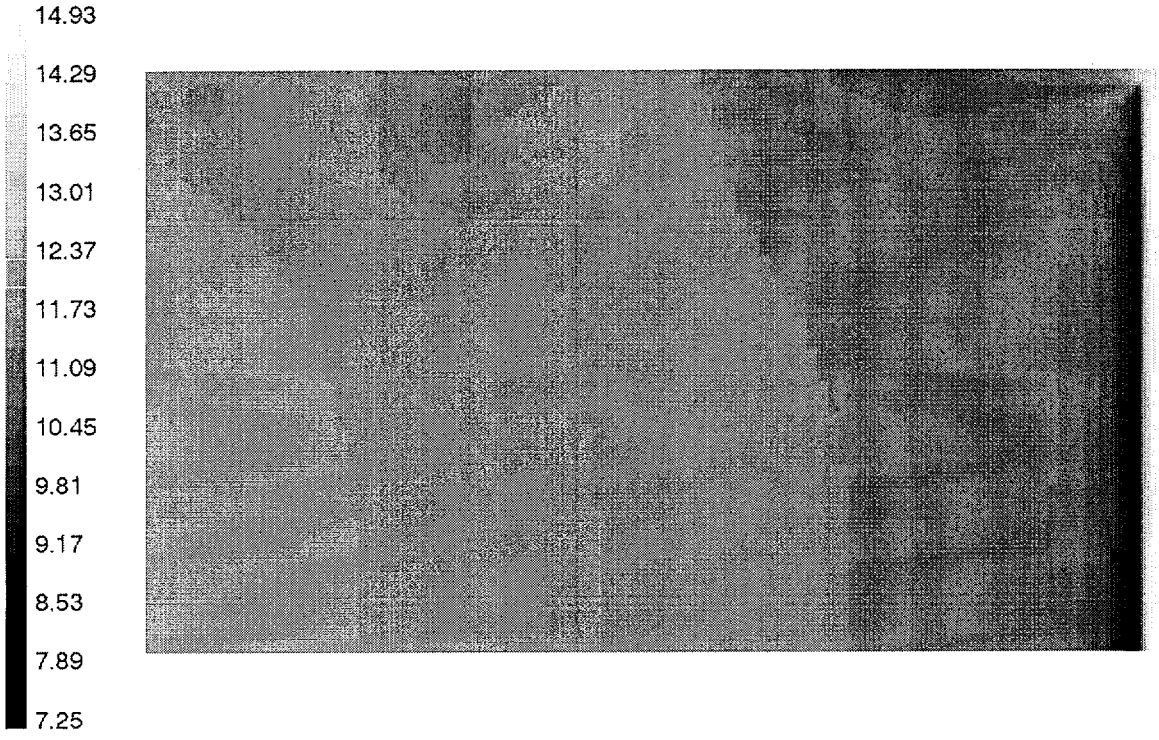

Figure 12. Pressure Contours Below the Fuel Racks, Pa (z = 0.1 m)

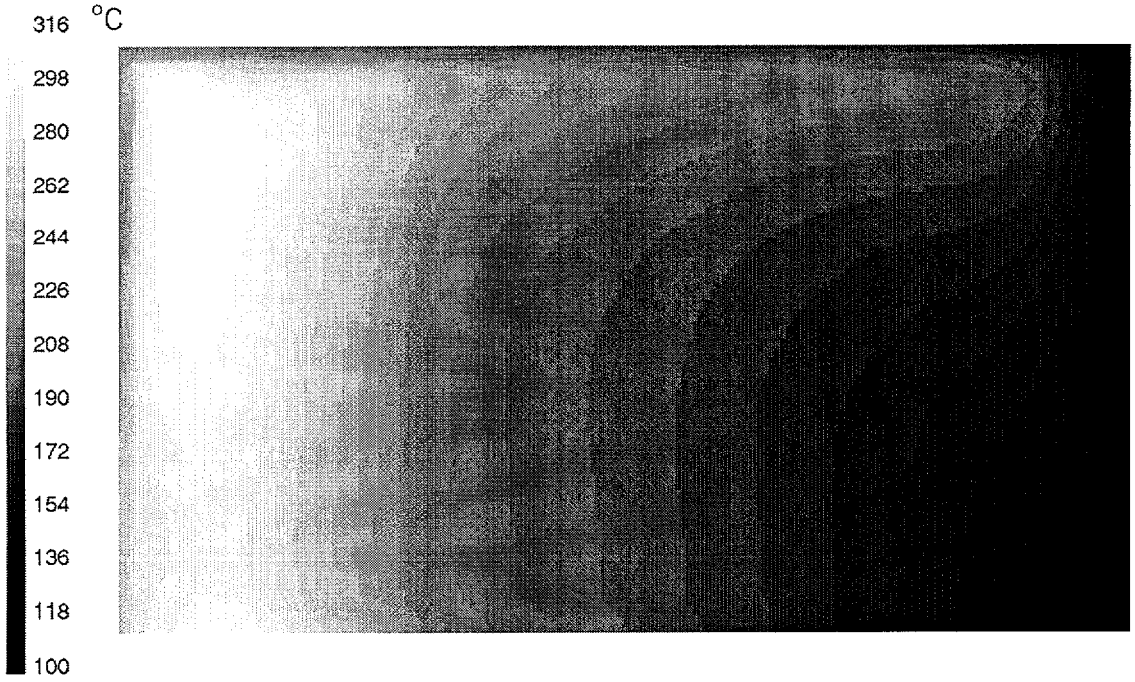

Figure 13. Temperature Contours Above the Fuel Racks (z = 4.5 m)

Figure 14. Temperature Contours Below the Fuel Racks (z = 0.1m)

Temperature contours above the fuel racks (Fig 13.) are consistent with the description of the flow paths given earlier. The stagnation region on the symmetry plane near the right side downcomer has the lowest temperature. This is a result of the cold plume falling into the pool region and stagnating on the racks at this point (see Figure 7). As the flow travels across the racks to the left, it mixes with hotter air exiting the racks. This increase in temperature is clearly seen in Figure 13. The rising hot plume on the left side of Figure 13 is the hottest region at this level. This area roughly covers the hottest fuel region (f1). The average temperature above the racks at this level is 217 °C. This value is computed over a series of iterations to get a representative value. The spatial variation in temperature at this level is roughly 200 degrees.

Figure 14 shows the temperature contours below the fuel racks. The average temperature for this level is 137 °C. The spatial variation in temperature is nearly 60 degrees. Most of this spatial variation is accounted for by the hot spot near the top right hand corner of Figure 14. This region is caused by a small downflow predicted to occur in the fuel racks in the cells just above this region. This downflow is heated by the fuel before it enters the region below the racks.

The temperature below the racks is nearly equal to the containment outlet vent temperature. This feature of these predictions is coincidental. There is a 30 degree average temperature difference between the floor and ceiling in the containment. The outlet vent is near the ceiling and is exposed to the hotter layers of air in the containment. The air which cools the fuel comes mainly from the floor of the containment. As it travels to the region below the racks, it rises in temperature to nearly equal the outlet vent temperature.

7.2 Tabulated Results for Each Case

The predicted values for each of the case studies described in Table 3 are outlined in Tables 6, 7, and 8. Table 6 lists relevant temperatures and pressures. Table 7 summarizes mass flow rates through the fuel region. Table 8 is a summary of the global energy balance for each case. Each of the tabulated results represents an average value. The solutions are predicted to be naturally unsteady. Averages are obtained from approximately 1000 iterations recorded once the solution reaches a steady state pattern. The magnitude of the variation in depends upon the variable considered. The results for each sensitivity study are discussed following the tables.

Table 6. Predicted Temperatures and Pressures

case ID	max T (°C)	T at outlet (°C)	Average T (°C)		Average P (Pascal)	
			above rack	below rack	above rack	below rack
f2v2h0	1047	176	297	177	18.9	15.2
f3v2h0	686	148	245	149	17.5	13.3
f4v2h0	537	133	217	137	16.7	11.8
f6v2h0	445	120	193	128	16.1	10.7
f4v1h0	954	237	309	259	6.5	2.9
f4v1p5h0	642	167	254	171	11.1	7.3
f4v2p5h0	518	112	186	123	23.1	16.6
f4v2h2	527	102	174	113	14.9	9.5
f4v2h4	477	91	171	111	14.0	6.7
f4v2h0rp	586	133	218	135	16.8	12.1
f4v2h0rm	519	133	216	139	16.7	11.4
f4mv2h0	567	133	212	138	16.4	12.1
f4v2h0km20	543	133	215	137	16.7	11.6
f4v2h0km50	570	133	207	140	16.7	11.9
f4v2h0b50	712	160	268	163	18.0	13.5
f2v2h2	847	134	243	143	16.5	13.0
f3v2h2	595	114	202	125	15.5	11.5
f6v2h2	392	94	167	100	14.4	9.1

Table 7. Predicted Mass Flow Rates

case ID	inlet (kg/s)	flow rate through fuels (kg/s)					downcomer flow (kg/s)			
		f1	f2	f3	f4	net	left	rear	right	net
f2v2h0	5.18	.35	.11	.11	.81	1.39	.22	-.14	-1.46	-1.38
f3v2h0	5.18	.40	.13	.12	.90	1.55	.25	-.26	-1.53	-1.54
f4v2h0	5.18	.41	.13	.12	.89	1.54	.22	-.18	-1.58	-1.54
f6v2h0	5.18	.39	.13	.12	.92	1.56	.22	-.20	-1.57	-1.56
f4v1h0	2.59	.20	.07	.07	.74	1.09	-.99	-.33	.23	-1.08
f4v1p5h0	3.88	.36	.11	.11	.84	1.42	.17	-.17	-1.41	-1.41
f4v2p5h0	6.47	.42	.13	.12	.87	1.54	.31	-.2	-1.65	-1.54
f4v2h2	5.18	.44	.14	.13	1.09	1.79	.17	-.48	-1.48	-1.79
f4v2h4	5.18	.45	.14	.13	.93	1.64	.33	-.31	-1.65	-1.63
f4v2h0rp	5.18	.36	.12	.11	.83	1.42	.19	-.05	-1.55	-1.41
f4v2h0rm	5.18	.45	.14	.13	.96	1.68	.31	-.40	-1.58	-1.68
f4mv2h0	5.18	.38	.13	.10	1.04	1.65	.04	-.19	-1.50	-1.65
f4v2h0km20	5.18	.40	.13	.12	.88	1.53	.26	-.23	-1.55	-1.52
f4v2h0km50	5.18	.40	.13	.12	.90	1.55	.30	-.37	-1.47	-1.55
f4v2h0b50	5.18	.37	.12	.11	.89	1.45	.18	-.13	-1.53	-1.48
f2v2h2	5.18	.46	.15	.14	1.12	1.87	.30	-.87	-1.28	-1.86
f3v2h2	5.18	.49	.16	.15	1.18	1.97	.34	-.97	-1.33	-1.97
f6v2h2	5.18	.45	.14	.14	1.09	1.82	.19	-.28	-1.72	-1.81

Table 8. Predicted Global Energy Balance Terms

case ID	Heat Load from Fuel (kW)					Convected enthalpy	Heat transfer at walls
	f1	f2	f3	f4	net		
f2v2h0	368.0	71.6	50.9	288.0	778.4	-778.4	0
f3v2h0	248.0	55.9	45.5	283.7	633.2	-633.2	0
f4v2h0	184.8	48.1	40.6	278.0	551.5	-551.5	0
f6v2h0	136.4	39.5	36.3	272.2	484.5	-484.5	0
f4v1h0	184.8	48.1	40.6	278.0	551.5	-551.5	0
f4v1p5h0	184.8	48.1	40.6	278.0	551.5	-551.5	0
f4v2p5h0	184.8	48.1	40.6	278.0	551.5	-551.5	0
f4v2h2	184.8	48.1	40.6	278.0	551.5	-395.1	-156.4
f4v2h4	184.8	48.1	40.6	278.0	551.5	-338.9	-212.6
f4v2h0rp	184.8	48.1	40.6	278.0	551.5	-551.5	0
f4v2h0rm	184.8	48.1	40.6	278.0	551.5	-551.5	0
f4mv2h0	184.8	48.1	40.6	278.0	551.5	-551.5	0
f4v2h0km20	184.8	48.1	40.6	278.0	551.5	-551.5	0
f4v2h0km50	184.8	48.1	40.6	278.0	551.5	-551.5	0
f4v2h0b50	230.4	61.0	52.1	352.6	696.0	-696.0	0
f2v2h2	368.0	71.6	50.9	288.0	778.4	-563.2	-215.2
f3v2h2	248.0	55.9	45.5	283.7	633.2	-458.6	-174.6
f6v2h2	136.4	39.5	36.3	272.2	484.5	-352.2	-132.3

7.3 Decay Time Sensitivity, Adiabatic Walls

The primary sensitivity study focuses on the decay time, defined as the time since reactor shutdown. As decay time increases, the heat load from the fuel decreases. Decay times of 2, 3, 4, and 6 years are studied. The physical and numerical conditions are identical for each case. Only the decay time is varied. Each case is based upon an assumed burnup of 40 GWd/MTU. Predicted temperatures are plotted in Figure 15. Spline fits connect the data. The maximum temperature decreases significantly (511 °C) between 2 and 4 years. From 4 to 6 years, the drop in temperature is only 91 °C. The shape of this curve closely resembles the decay heat curve. It is important to keep in mind the limitations (noted earlier) of these predictions at elevated temperatures. The 2 and 3 year results reach temperatures where the lack of radiation and chemistry models is expected to affect the solution.

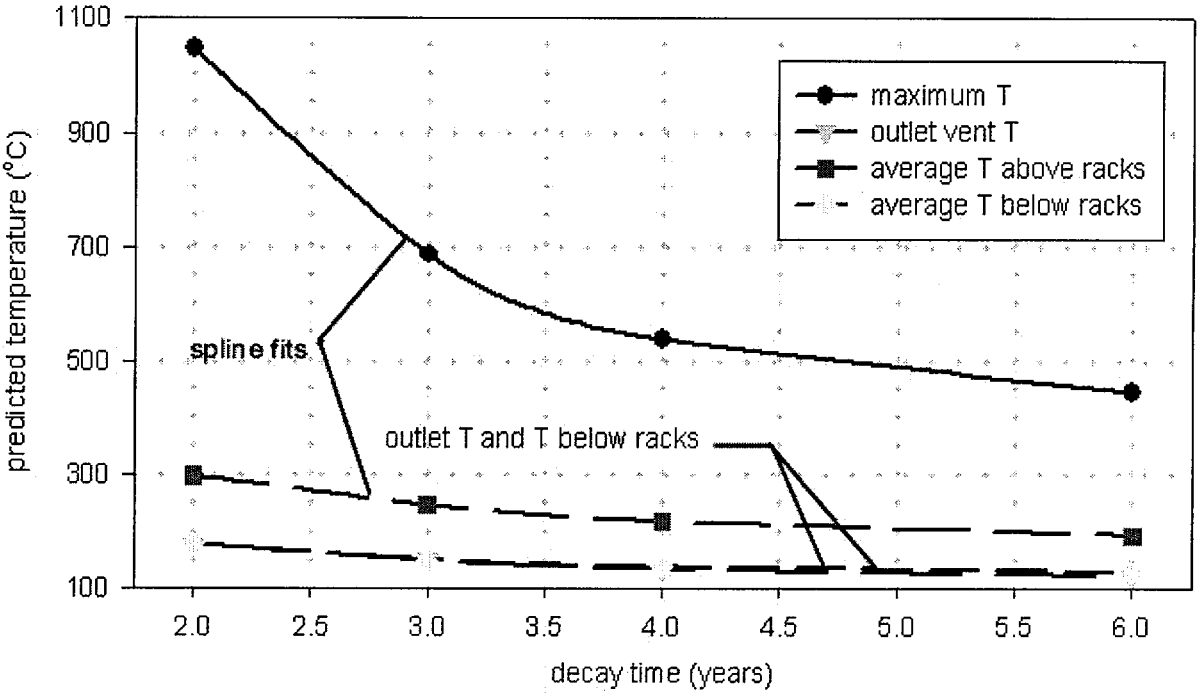

Figure 15. Predicted Temperatures vs. Decay Time, Adiabatic Walls

Temperatures above and below the rack differ by nearly 80 °C. These temperatures decline with decay time as expected. The rate of decline also decreases significantly after 4 years. The outlet vent temperature is predicted to decline in the same manner. One unexpected prediction is the near match between the outlet temperature and the average temperature below the racks. This coincidental result is discussed in a previous section.

The average pressure above and below the racks shows a slight increase as the decay time decreases. This is mainly because the pressure drop at the outlet vent increases as the decay time decreases. The outlet vent is at the end of a 4 m convergent duct protruding out from the containment wall. The pressure drop in this duct increases with the increase in viscosity and velocity associated with lower decay times. The increase in flow resistance through the outlet duct slightly increases the global containment pressure.

The flow patterns for the 2, 3, 4, and 6 year cases are qualitatively the same. Downcomer flows are predicted to distribute in a similar manner. The left downcomer has a slight upflow for each case. The rear downcomer has a similar net downflow. Cooling flow enters the region below the racks mainly through the right downcomer. No clear trend with decay time is observed. The prediction of less total mass flow for the 2 year case is unexpected. The 2 year case does show larger velocities in the fuel region. The decrease in density, however, results in less total mass flow. The increased temperature associated with the 2 year case results in an increase in viscosity. The increased viscosity and velocity in this case increases the pressure-loss terms for flow through the racks. This factor is assumed to be partly responsible for the decreased mass flow associated with the 2 year case.

Flow through each of the fuel regions shows a similar pattern. No clear trend is observed with decay time variation. The noticeable exception is the reduced flow rate predicted for the 2 year case. Predictions for the 3, 4, and 6 year cases show nearly identical flow rates through each of the fuel types. The similar flow rates indicate that the increases in velocity for the lower decay times (higher T) are offset by similar decreases in density.

7.4 Ventilation Rate Sensitivity

An important input parameter is the ventilation rate. The base ventilation rate assumes 2 building volumes of cool air enter the building each hour. Additional predictions are made with 1, 1.5, and 2.5 building volumes per hour. Each case assumes a 4 year decay time and all external walls are adiabatic. Predicted temperatures are plotted in Figure 16.

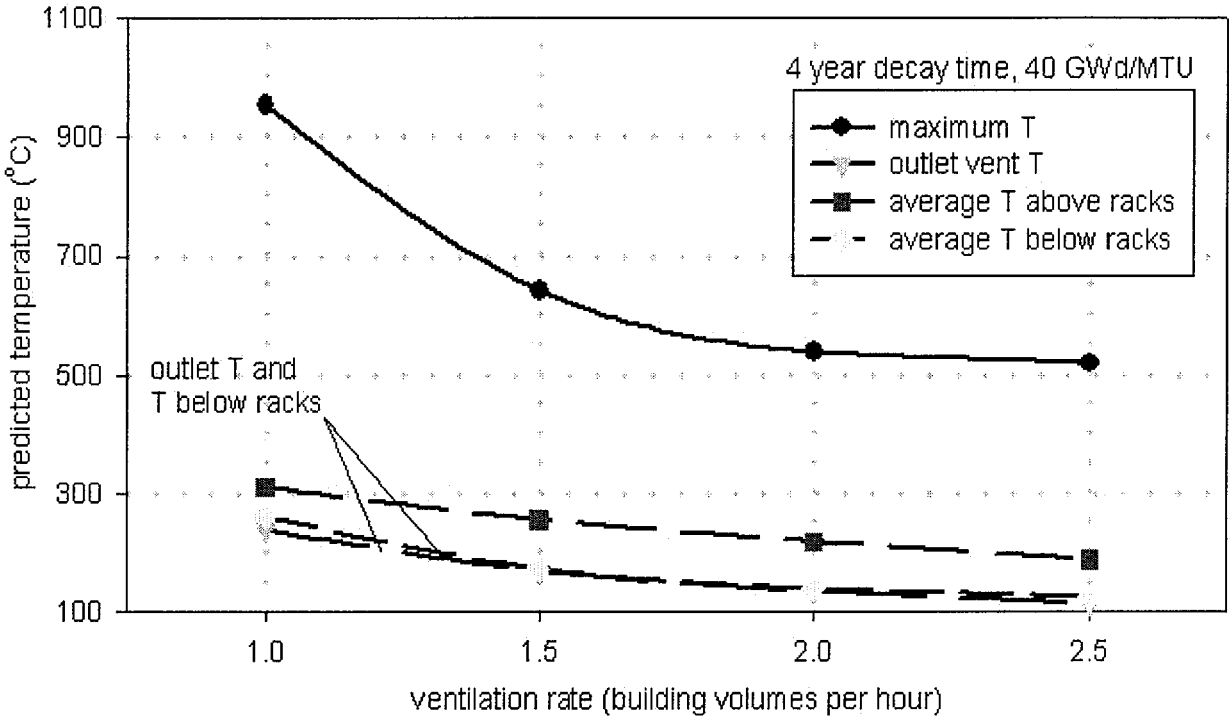

Figure 16. Sensitivity of Temperatures to the Ventilation Rate

The maximum temperature is significantly affected by the ventilation rate. The largest affect occurs when the ventilation rate is reduced from 1.5 to 1 building volume per hour. This trend suggests that reducing the ventilation rate below the 1 building per hour rate would significantly increase the temperature. This is not done because the model is not accurate at higher temperatures. The difference in the maximum predicted temperature between 2 and 2.5 buildings per hour is 19 °C. This is nearly equal to the difference in the predicted exit vent temperature for these two cases. It appears that the effect of increasing the ventilation rate beyond 2 buildings per hour can be approximated by globally adjusting the temperatures to the change in the outlet temperature determined from a global energy balance.

The pressure in the containment increases slightly as the flow rate increases due to increased pressure losses in the outlet vent. The difference in the average pressure between the upper and lower racks also increases with flow rate. This is attributed to the increased mass flow through the downcomer region and the associated increased pressure drop.

At the lower ventilation rate, the mass flow through the fuel drops off. The increased temperature reduces the density and this affects the mass flow. As the ventilation is increased, the mass flow through the fuel increases up to a point. No difference is observed in the mass flow rate through the fuel with the 2 and 2.5 building per hour ventilation rates. It appears that ventilation rates beyond 2 building volumes per hour don't significantly change the mass flow rates through the fuel or the net fuel temperature rise. The net fuel temperature rise is defined as the difference between the outlet vent temperature and the peak fuel temperature. Outlet vent temperature is considered a measure of the overall containment temperature.

7.5 Wall Heat Loss Sensitivity

A sensitivity study is done on the overall heat transfer coefficient between the containment and the exterior environment. Containment wall and ceiling heat transfer coefficients of 2 and 4 W/m^2-K are applied to the base 4 year case. Predicted temperature results are plotted in Figure 17. The temperatures drop predictably as the heat transfer coefficient is increased. The drop in the maximum predicted temperature is most significant when the coefficient is changed from 2 to 4 W/m^2-K. The temperatures above and below the racks respond differently. These temperatures change most dramatically when the heat transfer coefficient is changed from 0 to 2 W/m^2-K. The global energy balance also changes most when the coefficient is changed from 0 to 2 W/m^2-K.

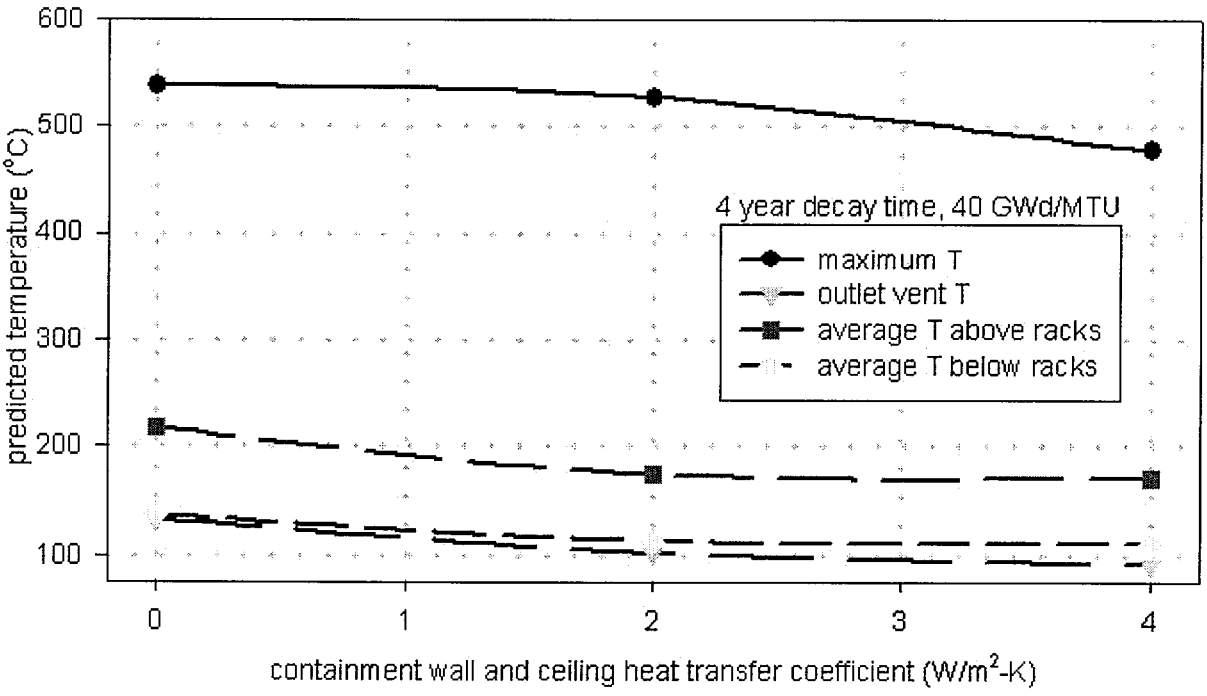

Figure 17. Sensitivity of Temperatures to Overall Heat Transfer Coefficient

The mass flow rates through the fuel region increase slightly as the heat transfer coefficient is increased. The limited data show no clear trend. The increase in the mass flow rate through the fuel is attributable to the lower containment temperatures resulting from the wall heat losses. The lower temperatures produce stronger natural circulation flows, which aid the fuel cooling.

The sensitivity of wall heat loss is also observed by comparing the adiabatic decay time sensitivity results (f2v2h0, f3v2h0, f4v2h0, f6v2h0) with the best estimate results (f2v2h2, f3v2h2, f4v2h2, f6v2h2). These models differ only by the wall and ceiling heat transfer coefficient which is set to 2 W/m^2-K in the best estimate predictions. The data are given in tables 6, 7, and 8. The most significant difference is the drop in peak temperature when the heat transfer coefficient is applied. This temperature reduction is greatest at the 2 year decay time due to the higher containment temperatures in this case. The peak temperature of the fuel drops by 200 °C when wall heat transfer is applied using fuel with a 2 year decay time. At 6 years decay time, the peak temperature drops by 53 °C when wall heat transfer is turned on. Temperatures at the outlet and above the fuel racks respond in a similar manner. No clear trend is observed in the average temperature computed below the fuel racks. Mass flow rates through the fuel and downcomers increase in the cases with wall heat transfer. This increased mass flow and reduced temperatures in the containment and fuel region account for the reduced peak fuel temperatures predicted.

7.6 Rack and Fuel Flow Resistance Sensitivity

The racks and fuel are modeled as a porous medium. The complexity of the physical structure in this area makes a detailed model impractical. A porous resistance is put into this region of the model to account for the viscous and inertial flow losses. Porous resistance is considered a significant parameter in these predictions. Details of the determination of the resistance coefficients are given in Appendix A. There is some uncertainty in the data used to determine the loss coefficients, and there are a variety of rack and fuel bundle designs that affect the flow loss. This sensitivity study shows the effect of flow loss variations on the predicted temperatures.

Using the base case as a starting point, two additional predictions are done with the resistance coefficients changed by +/- 20%. The increased resistance reduces the mass flow rate which increases the temperature rise of the air flowing through the racks. Similarly, with less resistance the mass flow is increased and the temperature rise is reduced as the data in Table 7 demonstrate. Figure 18 shows the predicted temperature for these cases. The maximum temperature increases with the increased resistance, as expected. This trend is attributable to the mass flow rates discussed above. The largest change occurs when the resistance is increased by 20%. The building outlet temperature is unaffected since the overall energy balance is unchanged. The average temperatures above and below the racks show no significant change.

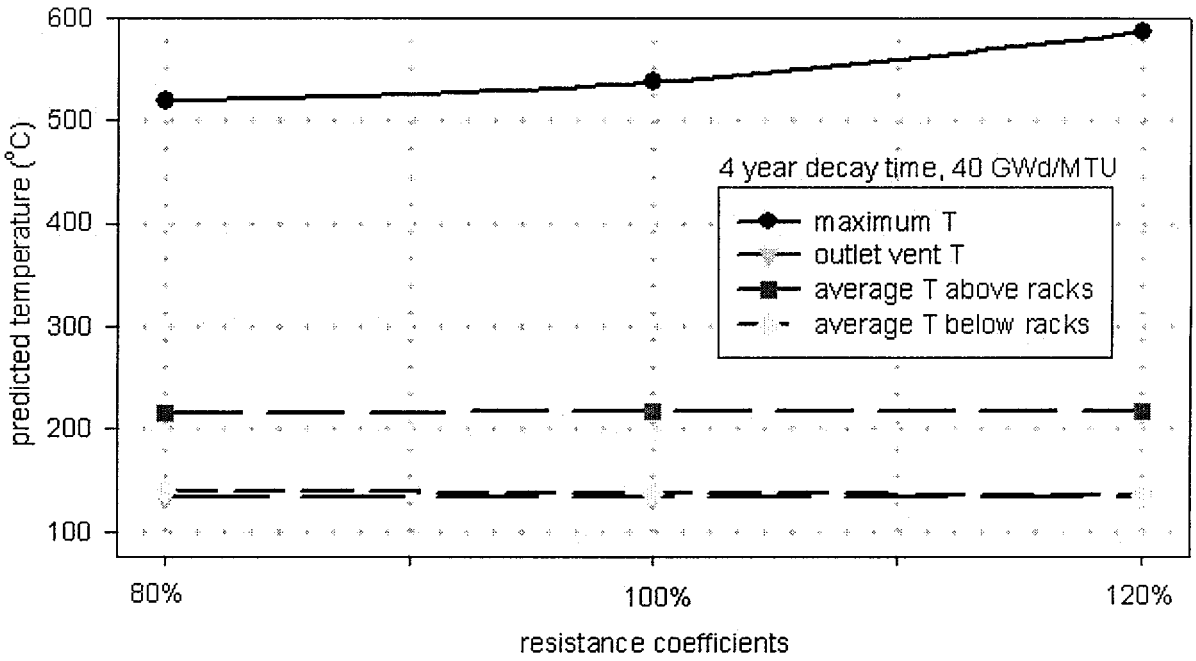

Figure 18. Sensitivity of Temperatures to Flow Resistance

7.7 Hottest Fuel Location Sensitivity

The hottest fuel is placed along the left wall of the fuel pool for each of the predictions described above. The hottest fuel represents the last fuel taken from the reactor when the reactor is shut down. The fuel pool is assumed to be filled from right to left (Figure 1), so that the last fuel taken from the reactor is on the left. As a sensitivity study, the hottest fuel is moved to the center of the pool. Fuel region f2 is next to the hottest fuel on the left. Fuel region f3 is to the right of the hottest fuel. The remaining rack locations are filled in with the oldest fuel, f4. The total fuel load and quantities of each type of fuel are unchanged by this arrangement.

The most conservative (hardest to cool) location for the hottest fuel is not obvious. Placing the hottest fuel in the center of the pool puts the fuel farthest from the downcomer regions supplying the cooling air flow, which could make it harder to cool. However, placing the hottest fuel next to the downcomer can block the cooling air from flowing down through this downcomer. This blockage can result from the rising hot plume. There is no benefit to putting the hot fuel next to a downcomer in this case. Two fuel positions are compared here to show the effect of fuel position on the predicted results.

The base case assumes the hot fuel is along the left wall, as described above. Downflow to the left downcomer is blocked off by the rising plume. A small upward flow is established in this downcomer by entrainment and other factors. Cooling air from the right downcomer travels along the pool floor under the racks to reach the hottest fuel (see Figure 10). The average peak temperature in the fuel region is 537 °C.

The predictions done with the hottest fuel in the center of the pool are very similar to the base case predictions described above. The hot plume that rises from the center of the pool is swept to the left wall of the pool before rising into containment. The pattern is similar to Figure 6. Cold inlet air falls to the floor of the containment and travels around the pool, as shown in Figure 8. The average maximum temperature in the fuel region for this case is 567 °C. The mass flow rate through the hottest fuel is slightly smaller when this fuel is in the center of the pool. The inlet flow path apparently affects the flow patterns in the fuel pool.

7.8 Rack and Fuel Thermal Conductivity Sensitivity

The racks and fuel are modeled as a porous medium because of the physical structure in this area is too complex to model. This porous model requires the user to specify properties to account for given thermal behavior. The thermal property assumptions are given in Appendix B. The thermal properties of the porous medium affect the thermal inertia and the conduction flux in the porous region. Thermal inertia is only a factor in transient terms so it is not expected to affect the steady-state results. The thermal conduction term, however, does move fuel energy away from the hottest regions. Thermal conductivity is approximated by assuming one-dimensional conduction in the vertical direction. The FLUENT code assumes isotropic thermal conductivity. The isotropic assumption used by the code and the one-dimensional assumption used to approximate the thermal conductivity are both questionable assumptions. The base case thermal conductivity is reduced by 20% and 50% in separate predictions to quantify the sensitivity of the results to this input parameter.

The maximum temperature increases slightly as the thermal conductivity of the porous medium decreases (See Table 6). The reduction in thermal conductivity slows the conduction of heat away from the hottest regions and accounts for this increase. The maximum predicted temperature increases by less than 30 °C as the thermal conductivity in this region is reduced by 50%. This is considered a weak sensitivity. The global flow patterns, the integrated mass flow through the fuel regions, and the global energy balance are not significantly affected by changing the porous thermal conductivity.

7.9 Fuel Burnup Sensitivity

All predictions are done assuming an average fuel burnup of 40 GWd/MTU. A sensitivity study is done using an average fuel burnup of 50 GWd/MTU and a decay time of 4 years. The higher fuel burnup assumption, when applied in this model, increases the energy generation term in the fuel region. The energy associated with a fuel burnup of 50 GWd/MTU is summarized in Table 1. The total pool energy at 4 years for the 50 GWd/MTU burnup falls between the 2 and 3 year cases with a burnup of 40 GWd/MTU.

The predicted temperatures and pressures reported in Table 6 for the higher burnup case fall between the 2 and 3 year cases, which use a burnup of 40 GWd/MTU. This is consistent with the observation noted above concerning the total pool energy. The mass flow rate predictions from Table 7 also generally fall between the 2 and 3 year cases. Similar to the other cases, the majority of the cooling flow travels down the right hand downcomer to the region below the racks. The average maximum temperature in the fuel region for this case is 712 °C.

7.10 Best-Estimate Critical Decay Time

Predictions are made at each of the four decay times using best-estimate parameters. These parameters include an overall wall heat transfer coefficient of 2 W/m^2-K and a ventilation rate of 2 building volumes per hour. These results represent the best estimate of the fuel temperatures and the convective flowfields, given the assumptions and limitations of this model. The difference between these results and the decay time sensitivity results (outlined in section 7.3) is the heat transfer coefficient on the building walls and ceiling. The heat loss from the walls and ceiling lowers the temperatures compared to the adiabatic decay time sensitivity outlined in section 7.3 of this report. The general features of the solution remain unchanged.

The primary result is the decay time sensitivity given in Figure 19. The data from cases f2v2h2, f3v2h2, f4v2h2, and f6v2h2 are plotted. Critical decay times of 26 and 35 months are noted on the figure for temperature limits of 800 °C and 600 °C, respectively. Critical decay time is defined as the post shutdown time required to ensure fuel temperatures don't rise above predefined temperature limits after a complete loss of fuel pool coolant. The 26 month decay time, associated with the 800 °C temperature limit, has significant uncertainty due to the model limitations at elevated temperatures discussed earlier. More details of these results are discussed earlier in this report and the principal data are outlined in Tables 6, 7, and 8.

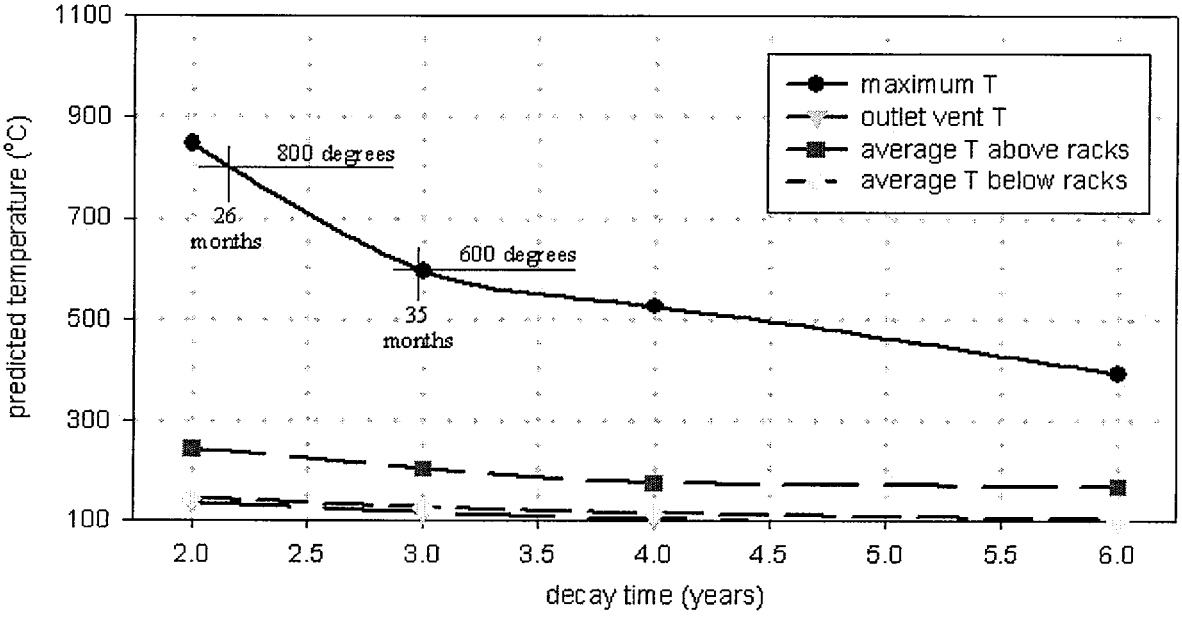

Figure 19. Best-Estimate Results for Maximum Temperature vs. Decay Time

8 SUMMARY

In support of the NRC rulemaking activity related to decommissioning, the Office of Research is using the FLUENT CFD code to study the air cooling phenomena of a spent fuel storage pool after a complete pool drainage. This study provides a solution for the critical decay time of a BWR spent fuel pool configuration. A series of sensitivity studies are completed to show the significance of some of the assumptions and parameters used to complete the predictions.

This study focuses on the potential modeling limitations of previous spent fuel heatup predictions which relied on simplified flowfield models. This three-dimensional CFD treatment avoids the need for many flowfield assumptions in the fuel and rack region. These results give significant insights into the spent fuel pool cooling issue. The natural circulation flows predicted are the most significant factor in removing heat from the fuel under these conditions. These results help reduce the uncertainty associated with this most significant aspect (natural circulation flows) of spent fuel pool cooling. However, the model does not include terms for the radiation and exothermic cladding reactions. These terms are significant at temperatures greater than approximately 600 °C. The present predictions form one piece of an overall solution to this issue. When using these predictions, the assumptions and limitations must be considered.

The series of predictions completed form a database of results which help define the natural circulation flows associated with this spent fuel cooling scenario. These results provide a basis for determining the applicability of the simplified flowfield assumptions used in codes such as COBRA-SFS, SFUEL, and SHARP. The simplified constant temperature and pressure boundary conditions used in previous studies can be assessed using the quantitative pressure and temperature variations predicted in this study. The basis for the boundary temperatures and pressures applied in these codes can also be re-considered in light of the results obtained here. Sensitivity studies using these codes can be guided by the results and sensitivities of this current study. Sensitivity studies and analysis with these simplified flowfield models are beyond the scope of this report which focuses solely on the CFD model and predictions.

A similar global flow pattern is predicted for most of the solutions. The primary flow travels down around the fuel racks and then up through the hot fuel. A hot plume rises from the pool to the containment ceiling and exits through the outlet vent. Temperatures, pressures, velocities, and mass flow rates are recorded for a series of cases designed to quantify the effect of important input parameters. Quantitative results are tabulated and compared. The peak temperature is the predicted result of greatest interest.

The primary sensitivity study focused on the critical decay time. The maximum predicted temperature drops with decay time along a curve similar to a decay curve. Using adiabatic containment walls, the maximum predicted temperature is 800 °C at approximately 32 months decay time. Maximum predicted temperature is 600 °C at 40 months. Using the best-estimate wall heat transfer coefficient on the containment walls and ceiling, the critical decay times for the 800 and 600 °C temperature limits are 26 and 35 months, respectively. The 800 and 600 °C limits are reference points only. Determination of appropriate critical temperature limits is beyond the scope of this report.

Containment ventilation significantly affects the predictions. Increasing ventilation rates beyond the baseline of 2 building volumes per hour has an insignificant effect. Decreasing the ventilation rate to 1 building volume per hour increases the predicted peak temperature by over 400 °C. For a given fuel decay and burnup, the ventilation rate is the most significant parameter in this study. These results are completed with adiabatic containment walls.

The heat transfer coefficient on the containment wall is varied from 0 to 4 W/m^2-K. A value of 2 W/m^2-K is used for best-estimate predictions. The variations in the heat transfer coefficient at 48 months decay time causes the peak predicted temperature to drop by 60 °C as the overall

heat transfer coefficient is increased from 0 to 4 W/m^2-K. A larger temperature change is predicted at shorter decay times, where the containment temperatures are higher.

Porous resistance and thermal conductivity are parameters computed by hand for use in the model. These parameters are varied to quantify the effect of their uncertainties on the final predictions. Varying the flow resistance in the racks up and down by 20% resulted in temperature changes of 49 and -18 °C, respectively. Reducing the expected thermal conduction parameter in the fuel racks by 50% increased the peak predicted temperature by 33 °C. These variations are minor compared to the effect of other input parameters in the model.

The decay curve used in this study assumed an average fuel burnup of 40 GWd/MTU. A sensitivity study completed with 50 GWd/MTU at 4 years decay time increased the peak temperature by 175 °C. The increased burnup significantly increases fuel power. The increase in temperature associated with the higher burnup fuel is consistent with the increased fuel heat load. Fuel burnup is a significant parameter in these predictions.

9 REFERENCES

1. Nourbakhsh, H.P., et al, "Analysis of Spent Fuel Heatup Following Loss of Water in a Spent Fuel Pool, A Users Manual for the Computer Code SHARP," NUREG/CR-6441, May 1998.

2. Benjamin, A.S., et al., "Spent Fuel Heatup Following Loss of Water During Storage," NUREG/CR-0649, March 1979.

3. Sailor, V.L., et al., "Severe Accidents in Spent Fuel Pools in Support of Generic Safety Issue 82," NUREG/CR-4982, July 1987.

4. Fluent Inc., "Fluent 5 Users Guide," Canterra Resource Park, 10 Cavendish Ct, Lebanon, NH 03766, 1998.

5. Anderson, J.D., *Computational Fluid Dynamics: The Basics with Applications*, McGraw-Hill Series in Mechanical Engineering, McGraw Hill, 1995.

6. ASHRAE, "*Handbook of Fundamentals*", 1981.

7. White, F.M., *Viscous Fluid Flow*, Mc Graw Hill, 1991.

8. Todreas, N.E., Kazimi, M.S., *Nuclear Systems I: Thermal Hydraulic Fundamentals*, Hemisphere Publishing Corporation, 1990.

APPENDIX A
LOSS COEFFICIENTS FOR FLOW THROUGH BWR FUEL STORAGE RACKS

A.1 BACKGROUND

The computational fluid dynamics (CFD) analysis of spent fuel pool cooling documented in this report uses a porous medium to represent the racks and fuel. The porous model allows the user to input flow resistance coefficients to represent viscous and inertial flow losses in the region. The porous medium represents the effect of the racks and fuel on the flow, without the need to represent the precise geometry of the fuel and racks. This analysis is done with the FLUENT CFD. FLUENT's porous model adds a source term to the momentum equations to account for viscous and inertial flow losses in the porous regions. The physical flow area is not changed so the fluid does not accelerate. Equation A-1[1] gives the FLUENT source term in one dimension. The viscous term is first, followed by the inertial loss term.

$$dp/dx = D \cdot \mu V + C \cdot \tfrac{1}{2} \rho V \cdot |V| \qquad \text{eq A-1}$$

In three dimensions, the coefficients D and C represent matrices. These values are input parameters for the FLUENT porous media model. This appendix gives background information and assumptions used in determining D and C in the form required for the FLUENT model.

A.2 GEOMETRY

Fuel bundles are stored in the spent fuel pool in racks that keep the bundles upright and provide neutron absorption. In this analysis, a high-density rack is filled with 9x9 BWR spent fuel bundles. The bundle characteristics are typical for a BWR.

Figure A-1 shows a BWR high-density rack. The square boxes composing the rack are 0.154 m (6.06 in.) from center to center. Rack height (w/o legs) is assumed to be 4.3 m (14.1 ft). The active fuel length is 3.8 m (12.45 ft) and is assumed to be centered in the rack from top to bottom. Rack distance from the floor is 0.15 m (5.9 in.). The walls separating the fuel cells are solid. For the purposes of the CFD model, multiple racks are joined together to form a single rack of the type illustrated in Figure A-1. This single rack spans the entire pool. A gap of 0.15 m (5.9 in.) is modeled between the rack and each side wall of the pool. Every rack cell contains a complete 9x9 fuel bundle. The racks form a homogeneous nonisotropic structure whose properties can be defined by considering a single rack cell.

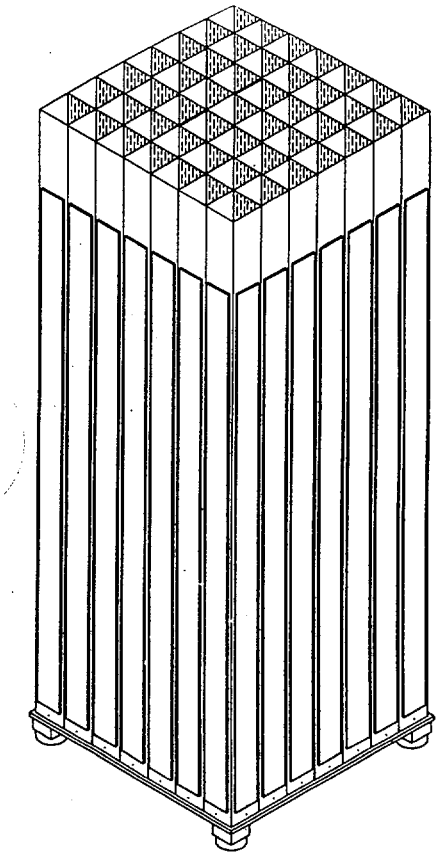

Figure A-1. High-Density Rack

Figure A-2 shows the cross section of a 9x9 fuel assembly in a fuel rack. The dark regions on each side are boral inserts in the rack structure. The rack cell pitch is 0.154 m (6.06 in.). The fuel bundle is contained in a channel box with an inner dimension of 0.134 m (5.3 in.). There is a gap between the rack walls and the fuel channel box. For the purposes of this analysis, all fuel rods are considered to be full length. The rod OD is 0.1118 m (.44 in.). Rod pitch is 0.1438 m (.566 in.). There are a total of 74 fuel rods and 2 water rods in the 9x9 cross-section. Table A-1 gives other values used to describe the geometry for the purposes of determining the loss coefficients. The left column in Table A-1 gives a convenient Identification for each value.

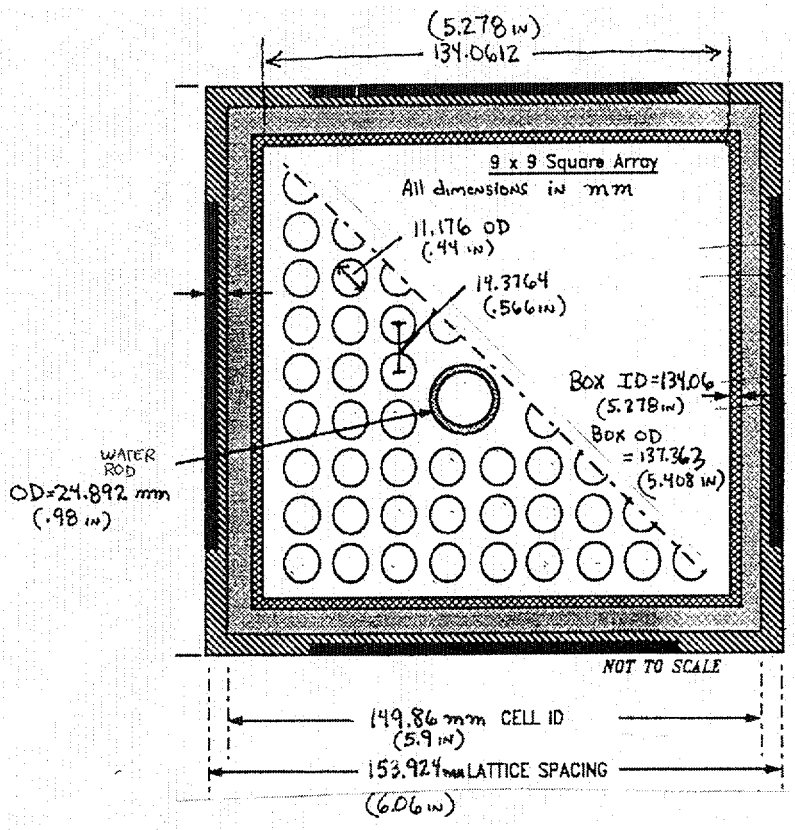

Figure A-2. Cross-Section of Rack and Bundle

Table A-1. Values Used to Determine Loss Coefficient in One Rack Cell

D1	Flow area available to FLUENT model	$(0.153924)^2 = 0.023692597$ m^2
D2	Channel box flow area (no rods)	$(0.1340612)^2 = 0.017972405$ m^2
D3	Channel box perimeter	4 x 0.1340612 = .5362448 m
D4	Cross-section area of rods (74 * π $d^2/4$)	0.007259294 m^2
D5	Cross-section area of water rods	0.000973283 m^2
D6	Perimeter of all rods (74 * π d) + (2 * π d_w)	2.75457357 m
D7	Total wetted perimeter (D3 + D6)	3.2908 m
D8	Total flow area (D2 - D4 - D5)	0.0097398 m^2
D9	Hydraulic diameter (4 A / P)= 4*D8/D7	0.0118388 m
D10	Flow area ratio at grid spacers	0.6 (area at spacers / area at tubes)
D11	Flow area ratio at tie plates	0.5 (area at tie plate / area at tubes)
D12	Lower orifice diameter (bottom of bundle)	0.09144m (3.6 in.)

A.3 LOSS COEFFICIENT DETERMINATION

The FLUENT code uses the loss coefficients, C and D, in equation A-1 to determine the momentum sink term used in the model. The velocity in equation A-1 represents the FLUENT solver velocity, which is the flow through the unobstructed flow area (D1 from table A-1). In reality, the velocity is higher for a given mass flow rate because of the reduced flow area of the physical structure (D8 in Table A-1). Figure A-3 shows a fuel bundle in a rack cell from the side. Viscous loss is accounted for along the tubes and side wall. The inertial losses are accounted for at the lower base hole, the lower and upper tie plates, and the seven grid spacers. Each of these losses is discussed below.

A.3.1 Viscous Loss

The viscous losses come primarily from flow along the tubes. It is assumed that viscous losses are uniform for the entire length of the racks. These losses are based on correlations for tube flow. Equation A-2 defines the pressure loss over a distance L along tube banks with hydraulic diameter d.

$$\Delta P_L = f \, {}^{L}\!/_{d} \left({}^{1}\!/_{2} \rho V^2 \right) \qquad \text{eq A-2}$$

The friction factor, f, is estimated[2] to be 96/Re. A value of 100/Re is used for this analysis. This is based on the flow along the tube bundles and the hydraulic diameter. Using the unobstructed velocity (V_F) from the FLUENT predictions, Equation A-2 is reduced to Equation A-3.

$$ {}^{dp}\!/_{dz} = 770231 \cdot \mu V_F \qquad \text{eq A-3}$$

The viscous loss term used in the FLUENT porous model is set to 770 x 10^3 / m^2.

A.3.2 Inertial Loss

Inertial losses are accounted for at the lower orifice (nose), the entrance into the tube region (at lower tie plate), the seven grid spacers, and the upper tie plate final expansion. Values for these coefficients are determined from References 2 and 3[3]. At the low Reynolds (Re) numbers expected in the simulation, the loss coefficients vary strongly with Re. The uncertainty in these numbers is large. The net effect, however, is not large, because the inertial losses are small compared to the viscous loss at low Re.

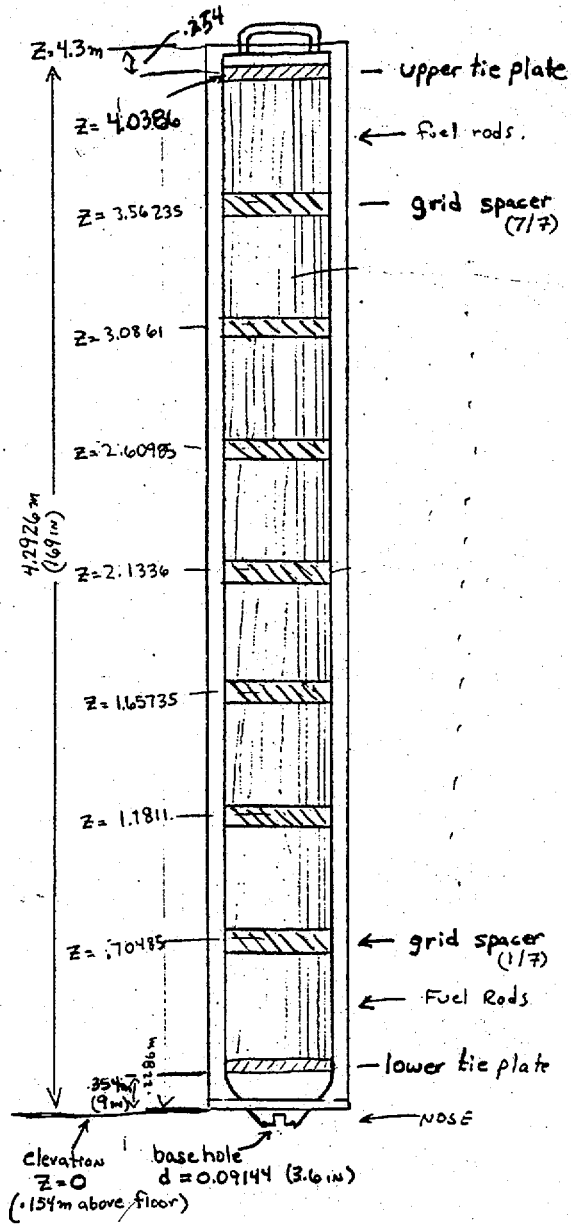

Figure A-3. Bundle Geometry (meters)

Table A-2 lists the parameters used to represent the inertial losses within the bundles. The 'k' is the k factor obtained from the reference material. In some cases, interpolations or even extrapolations are made to obtain this value. A representative value of k is used when k varies strongly with Re. Vr represents the reference velocity description associated with the k factor. The terms k_F and V_F represent the friction factor and velocity based upon the FLUENT model flow area (100% open). The value C needed by the code is also given. Note that the effect of C in the code is not a series of abrupt pressure drops at physical rack features, but an equivalent total pressure drop spread over the entire rack length L. The net effect of the inertial loss coefficients is given in the last row of Table A-2.

Table A-2. Inertial Loss Parameters

	k	**Vr based on**	**k_F**	**$C = k_F / L$**
Lower orifice	11	flow in open channel box	19.11	4.45
Entrance to tubes	1.2	flow along tubes	7.1	1.65
Grid spacers (1 of 7)	3.2	flow along tubes	18.94	4.4
Upper tie plate (w expansion)	4	flow along tubes	23.67	5.5
Effect of lower orifice, entrance to tubes, 7 grid spacers, and upper tie plate				**42.5 / m**

A.3.3 Final Code Input Summary

The FLUENT code input parameters which simulate the pressure drop through the rack and bundles are 770000 / m^2 for viscous losses and 42.5 / m for inertial losses. These values apply in the vertical direction. Lateral resistance is infinite due to the solid rack walls. Using infinite loss coefficients is not recommended in the FLUENT code. The lateral resistance values used in the model are set two orders of magnitude higher than the vertical coefficients defined above. This increased resistance and the several vertical walls used in the CFD model align the flow in the vertical direction.

A.4 COMPARISON WITH GE DATA

A plot of pressure loss through an 8x8 GE bundle is obtained for a quick comparison with the results obtained above. The GE data represent a single-phase pressure drop through a BWR bundle as a function of flow rate. It is unclear if the GE results are measured or computed. The results are at low Re numbers similar to the Re numbers expected in this analysis. Although the geometry for the 8x8 bundle is different from the 9x9 geometry, these results are considered a good indication of the appropriateness of the loss coefficients determined above. The pressure drop for two different flow rates is computed from the coefficients given above and compared to the GE data in Figure A-4. The agreement is good. Units are omitted from the figure to protect potential proprietary information.

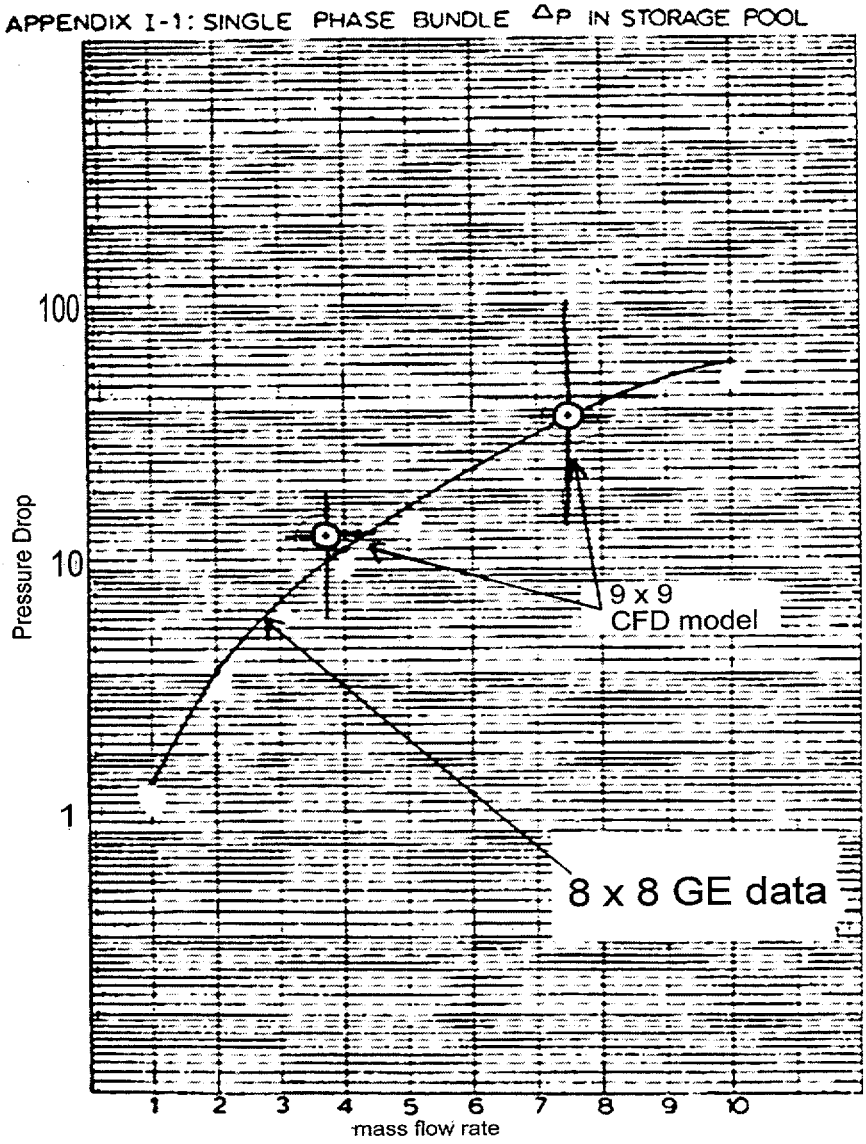

Figure A-4. Comparison With Predicted Pressure Drop of GE Data (Units dropped to protect potential proprietary data)

A.5 REFERENCES

1. Fluent Inc., "Fluent 5 Users Guide," Vol 1, p 6-104, Canterra Resource Park, 10 Cavendish Ct, Lebanon, NH 03766, 1998.

2. Todreas, N.E., Kazimi, M.S., *Nuclear Systems I: Thermal Hydraulic Fundamentals*, Hemisphere Publishing Corporation, 1990.

3. Idel'chik, I. E., "Handbook of Hydraulic Resistance," AEC-TR-6630, 1960.

APPENDIX B
THERMAL PROPERTY DETERMINATION FOR POROUS REGION REPRESENTING BWR FUEL AND STORAGE RACKS

B.1 BACKGROUND

The computational fluid dynamics (CFD) analysis of spent fuel pool cooling documented in this report uses a porous medium to represent the racks and fuel, dispensing with the need to represent the geometric details of the rack and fuel structure. The porous model allows the user to input thermal properties for the racks and fuel to represent the thermal conduction and thermal inertia in this region.

FLUENT's porous model uses an effective conductivity, as defined in equation B-1[1], to model the conduction in the porous media.

$$k_{eff} = \Phi k_f + (1 - \Phi) k_s \qquad \text{eq B-1}$$

The fluid conductivity (k_f) is augmented by the porous material conductivity (k_s). The porosity of the medium is represented by Φ. This appendix gives background information and assumptions used in determining k_s and Φ. The fluid conductivity is obtained from a table for the thermal conductivity of air (used throughout the model).

The thermal inertia term in the governing equations is also modified in the porous region to account for the properties of the solid material. Although thermal inertia only affects transient terms, its presence does stabilize the steady state solution. This appendix outlines the assumptions made to approximate the thermal inertia terms used in the FLUENT model.

B.2 GEOMETRY

The racks and fuel are considered a homogeneous nonisotropic structure whose properties are defined by considering a single rack cell. The cross-section of a single high-density rack cell with a 9x9 BWR fuel bundle is shown in Figure B-1. The dark regions on each side are boral inserts in the rack structure. The cell pitch is 0.154 m (6.06 in.). The fuel bundle is contained in a channel box with an inner dimension of 0.134 m (5.3 in.). There is a gap between the rack walls and the fuel channel box. For the purposes of this analysis, all fuel rods are considered to be full length. The rod OD is 0.1118 m (.44 in.). The rod pitch is 0.1438 m (.566 in.). There are 74 fuel rods and 2 water rods in the 9x9 cross-section. Table B-1 gives other values used to describe the geometry for the purposes of determining the loss coefficients.

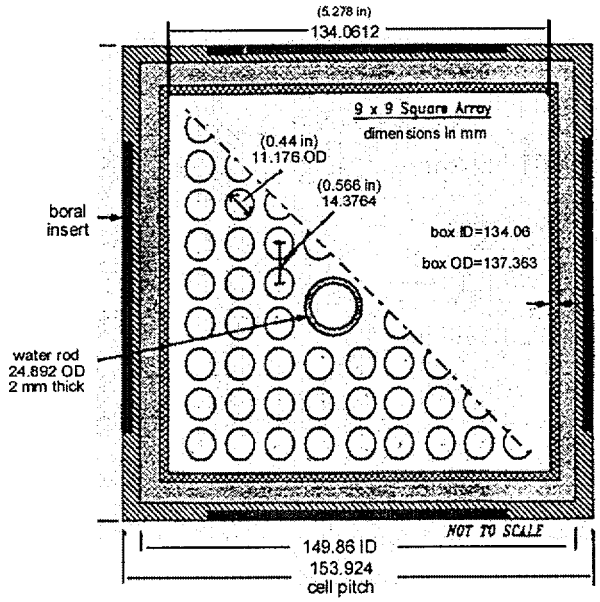

Figure B-1. Cross-Section of Bundle in Rack

The FLUENT code uses a single set of constant material properties and a porosity to account for the porous material. The rack and fuel structure in Figure B-1 is far more complex than the FLUENT model. For the purposes of this appendix, the rack and fuel are broken down into five regions according to material properties. The five regions are the rack, the air, the zirconium alloy, the fuel, and the boral inserts. Table B-1 lists the cross-sectional area (volume per meter length) and the thermal properties of the five regions.

Table B-1. Material Properties and Area of the Five Material Regions

Region	Area (m^2)	ρ (kg/m3)	Cp (J/kg-K)	k (W/m^2-K)
rack	0.000939	7800	580	23
air	0.013943	0.405 (600 °C)	1114 (600 °C)	0.061 (600 °C)
zirconium	0.002274	6500	330	13
fuel	0.006241	10970	247	3.6
boral	0.000319	2500	1500	18

Air, though included in the table, is not used in the analysis of thermal inertia. Its density is too low to have a measurable effect. Air is used in estimating the thermal conductivity but its effect is minimal. Properties for air are obtained from the table used in the FLUENT model for this case. Values at 600 °C are selected. This temperature is typical of the hottest fuel region in the racks. The rack is assumed to be stainless steel (Type 316). The steel properties come from Table 8-2 in Nuclear Systems I[2]. The fuel clad, water pipe, and channel box are assumed to consist of Zircaloy 2. Zircaloy properties are also obtained from Table 8-2 in Reference 2. The fuel (UO_2) properties are obtained from Table 8-1 in reference 2. The boral inserts are assumed to be boron carbide. The properties for this material are obtained from NUREG/ CR-6150[3].

B.3 THERMAL INERTIA

The thermal inertia term does not play a direct role in the final solution since it applies directly only to the transient terms. The final results are steady state. These terms do, however, help to stabilize the steady state results. Without this term, the fuel region temperature oscillations are very high due to the lack of thermal inertial in the model. For the purposes of estimating the thermal inertia, the transient term given by Equation B-2 is used.

$$(\Phi \rho_f \, Cp_f + (1-\Phi)\rho_s \, Cp_s) \, \partial T / \partial t \qquad \text{eq B-2}$$

Subscript f refers to the fluid (air) and subscript s refers to the solid. In this case, the solid is made up of several solids. The unknowns are Φ, ρ_s, and Cp_s. These unknowns are determined as a composite of the materials given in Table B-1. Equation B-3 is used to find these values.

$$(1-\Phi)\rho_s Cp_s = \sum_i \varphi_i \rho_i Cp_i \qquad \text{eq B-3}$$

Equation B-3 states that the thermal inertial of the sought-after solid is equivalent to the sum of the thermal inertia of the solids in the rack and fuel structure. The summation is over the four materials defined in Table B-1 (air is excluded). The term φ refers to the volume fraction of the particular material. The term ρ Cp refers to the thermal inertia of each of the materials. The data are summarized in Table B-2.

Table B-2. Thermal Inertia Terms

Region	% volume (φ)	ρ Cp V (J /K) (V is based on 1 m^3 total Volume)
rack	0.0396	179.1×10^3
zirconium	0.0959	205.7×10^3
fuel	0.2632	713.1×10^3
boral	0.0135	50.4×10^3
Summation	**0.4121**	**1148×10^3**

The summation on the right side of equation B-3 is equal to 1148×10^3 J/K. At this point there is a single equation with three unknowns. The unknowns are the porosity, density, and specific heat on the left side of equation B-3. The properties of steel are selected (arbitrarily) and the porosity is computed to yield the correct thermal inertia. This results in a porosity of 0.746, which is rounded to 0.75, then applied to the model.

Portions of the rack above and below the active fuel region do not have the same thermal inertia. As an approximation, the thermal inertia is computed assuming that the fuel and zirconium in Table B-2 are not present in these regions. Using the same material properties for the porous solid gives a porosity of 0.95 above and below the active fuel region. The thermal inertia parameters used in the model is given below.

B.3.1 Input Parameters for Thermal Inertia

- $\rho_s = 7800$ kg/m^3
- $Cp_s = 580$ J/kg-K
- $\Phi = 0.75$ (within the fuel region)
- $\Phi = 0.95$ (for the portion of the rack above and below the fuel)

B.4 THERMAL CONDUCTION

The thermal conduction plays a direct role in the final CFD model. This term directly influences a path of heat transfer away from the hottest fuel. A quick method is used to approximate this value, and sensitivity studies are done with the FLUENT model to quantify the effect of uncertainty in this input parameter.

To estimate the thermal conduction, the 1D parallel conduction resistance method is used. Equation B-4 defines the total resistance (R_T) in terms of the component resistances (R_i).

$$\frac{1}{R_T} = \sum \frac{1}{R_i}$$ eq B-4

Individual resistances are given by L/(k A). The term L is the distance in the conduction direction. The term k A is the thermal conductivity multiplied by the conduction area. Using the data from Table B-1 and assuming a length of 1 m gives a total resistance of 12.6. Using the total area of solids from Table B-1 (A_T = 0.009733 m^2), the effective conductivity can be computed from $R_T = 1/kA_T$. The effective conductivity is 8.12 for the solid region. This value also represents a simple volume-weighted thermal conductivity for the solid material regions.

The value computed for the effective thermal conductivity must be modified to account for the actual porosity used in the model. The term $\{(1-\Phi)\ k_s\}$ from equation B-1 is set equal to the conductivity found above and the porosity obtained by comparing the area fractions in Table B-1. The result is that the solid material thermal conductivity should be 13.4 for the porosity of 0.75 set earlier. The porosity and/or thermal conductivity values are not significant by themselves. It is the combination $\{(1-\Phi)\ k_s\}$ found in Equation B-1 that is significant. This appendix defines the porosity on the basis of the assumptions made in determining the thermal inertia terms. This porosity is carried through to the thermal conduction term since a region can only have one porosity. Even though the porosity value is not correct, the thermal conductivity is adjusted to yield the appropriate net effect. The thermal conduction parameters used in the model are given below.

B.4.1 Summary of Input Parameters for Thermal Conductivity

- k_s = 13.5 W/m-K (13.4 computed above; 13.5 used for model)
- Φ = 0.75 (in the fuel region)
- Φ = 0.95 (for the portion of the rack above and below the fuel)

B.5 REFERENCES

1. Fluent Inc., "Fluent 5 Users Guide," Vol 1, p 6-107, Canterra Resource Park, 10 Cavendish Ct, Lebanon, NH 03766, 1998.

2. Todreas, N.E., Kazimi, M.S., *Nuclear Systems I: Thermal Hydraulic Fundamentals*, Hemisphere Publishing Corporation, 1990.

3. SCDAP/RELAP5 Development Team, "SCDAP/RELAP5/MOD 3.2 Code Manual," NUREG/CR 6150, Vol. 4, Rev. 1, US Nuclear Regulatory Commission, Washington, DC 20555, Jul 1998.

NRC FORM 335 (2-89) NRCM 1102, 3201, 3202

U.S. NUCLEAR REGULATORY COMMISSION

BIBLIOGRAPHIC DATA SHEET

(See instructions on the reverse)

1. REPORT NUMBER (Assigned by NRC, Add Vol., Supp., Rev., and Addendum Numbers, if any.)

NUREG-1726

2. TITLE AND SUBTITLE

Predictions of Spent Fuel Heatup After a Complete Loss of Spent Fuel Pool Coolant

3. DATE REPORT PUBLISHED

MONTH	YEAR
June	2000

4. FIN OR GRANT NUMBER

5. AUTHOR(S)

Christopher F. Boyd

6. TYPE OF REPORT

Technical

7. PERIOD COVERED *(Inclusive Dates)*

8. PERFORMING ORGANIZATION - NAME AND ADDRESS *(If NRC, provide Division, Office or Region, U.S. Nuclear Regulatory Commission, and mailing address; if contractor, provide name and mailing address.)*

Division of Systems Analysis and Regulatory Effectiveness
Office of Nuclear Regulatory Research
U.S. Nuclear Regulatory Commission
Washington, DC 20555-0001

9. SPONSORING ORGANIZATION - NAME AND ADDRESS *(If NRC, type "Same as above"; if contractor, provide NRC Division, Office or Region, U.S. Nuclear Regulatory Commission, and mailing address.)*

Same as above

10. SUPPLEMENTARY NOTES

11. ABSTRACT *(200 words or less)*

This generic study was done to predict the peak fuel temperatures and flow patt erns observed after a complete loss of spent fuel pool coolant. The pool is assumed to be housed in a large containment bui lding with an operable ventilation path. Fuel temperatures and natural circulation phenomena are predicted using computationa l fluid dynamics (CFD). These predictions identify the peak temperatures and the principal flow paths and features of the natural convective cooling phenomena for the fuel pool and containment building. The model is representative of a typical BWR pool. The pool is filled to capacity with 4200 fuel bundles in high-density racking. Predictions are made with fuel load s representative of a fuel pool 2, 3, 4, and 6 years after reactor shut down. Sensitivity studies are done on the ventilation rate, the outer wall heat transfer, the location of the fuel, fuel burnup, the flow resistance, and heat conduction within the rack s. The FLUENT CFD code predictions show that fuel temperatures remain below the temperature limits of 800 oC and 600 oC afte r 26 and 35 months, respectively. In considering the quantitative results of this study, the limitations and modelin g assumptions must be kept in mind.

12. KEY WORDS/DESCRIPTORS *(List words or phrases that will assist researchers in locating the report.)*

spent fuel pool
complete loss of coolant
BWR
high density fuel racks
fuel temperature
natural circulation flow
decommissioning

13. AVAILABILITY STATEMENT

unlimited

14. SECURITY CLASSIFICATION

(This Page) unclassified

(This Report) unclassified

15. NUMBER OF PAGES

16. PRICE